Contrasting records of sea-level change in the eastern and western North Atlantic during the last 300 years

Long, A.J.[1*], Barlow, N.L.M.[1], Gehrels, W.R.[2], Saher, M.H.[2], Woodworth, P.L.[3], Scaife, R.G.[4], Brain, M.J.[1], Cahill, N.[5]

[1] Department of Geography, Durham University, South Road, Durham, DH1 3LE, United Kingdom

[2] Environment Department, University of York, Heslington, York, YO10 5DD, United Kingdom

[3] National Oceanography Centre, Joseph Proudman Building, 6 Brownlow Street, Liverpool L3 5DA, United Kingdom

[4] Department of Geography and Environment, University of Southampton, University Road, Southampton, SO17 1BJ, United Kingdom

[5] School of Mathematical Sciences (Statistics), University College Dublin, Belfield, Dublin 4, Ireland

*Corresponding author:

Antony Long

Email: a.j.long@durham.ac.uk

Telephone: +44 191 334 1913

Abstract

We present a new 300-year sea-level reconstruction from a salt marsh on the Isle of Wight (central English Channel, UK) that we compare to other salt-marsh and long tide-gauge records to examine spatial and temporal variability in sea-level change in the North Atlantic. Our new reconstruction identifies an overall rise in relative sea level (RSL) of c. 0.30 m since the start of the eighteenth century at a rate of 0.9 ± 0.3 mm yr^{-1}. Error-in-variables changepoint analysis indicates that there is no statistically significant deviation from a constant rate within the dataset. The reconstruction is broadly comparable to other tide-gauge and salt-marsh records from the European Atlantic, demonstrating coherence in sea level in this region over the last 150-300 years. In contrast, we identify significant differences in the rate and timing of RSL with records from the east coast of North America. The absence of a strong late 19^{th} / early 20^{th} century RSL acceleration contrasts with that recorded in salt marsh sediments along the eastern USA coastline, in particular in a well-dated and precise sea-level reconstruction from North Carolina. This suggests that this part of the North Carolina sea level record represents a regionally specific sea level acceleration. This is significant because the North Carolina record has been used as if it were globally representative within semi-empirical parameterisations of past and future sea-level change. We conclude that regional-scale differences of sea-level change highlight the value of using several, regionally representative RSL records when calibrating and testing semi-empirical models of sea level against palaeorecords. This is because by using records that potentially over-estimate sea-level rise in the past such models risk over-estimating sea-level rise in the future.

Key words: salt marsh, tide gauge, semi-empirical models, sea-level rise, English Channel

1. Introduction

Salt-marsh sea-level reconstructions can extend tide-gauge measurements back in time to create multi-century or millennia time series that may be compared with various forcing mechanisms, such as climate, ocean dynamics and ice sheet history. A key way to assess the reliability of these long-term records is to compare periods of overlapping salt-marsh data with tide-gauge measurements. Often the data agree (e.g. Gehrels et al., 2005) but in some instances they do not; for example, a study of 20th century sea-level rise using salt-marsh foraminifera from New Zealand's North Island reconstructed rates of sea-level rise that are about double that recorded at the nearby Auckland tide gauge (Grenfell et al., 2012).

On the east coast of the USA, where several late Holocene salt-marsh records exist (e.g. Donnelly et al., 2004; Gehrels et al., 2005; Kemp et al., 2009b; van de Plassche, 2000), comparisons with tide-gauge data are typically restricted to less than 100 years, with the longest tide-gauge record, that from New York, starting in AD 1856. Some of these salt-marsh records suggest a sea-level acceleration dated to the late 19th/early 20th century, several decades before the start of reliable tide-gauge data from the region. In the best dated and most precise reconstruction, from North Carolina, this acceleration is dated from a salt-marsh study as having taken place in the period AD 1865-1892 when the detrended (i.e. corrected for background glacio-isostatic adjustment (GIA)) rate of sea level increased by 2.2 mm yr^{-1}, from -0.1 mm yr^{-1} to +2.1 mm yr^{-1} (Kemp et al., 2011).

The five longest tide-gauge records in the world exist in northwest Europe (Liverpool, Brest, Amsterdam, Stockholm and Swinoujscie) with record lengths of between 200 and 300 years (Figures 1 and 2). Compared with the American salt-marsh records referred to above, these European tide gauges record a more gradual long-term acceleration in sea-level of about 0.01 mm yr^{-2} (Gehrels and Woodworth, 2013; Woodworth et al., 2011a; Woodworth et al., 2009; Woodworth et al., 2011b). Two European salt-marsh studies reconstruct RSL trends over the last 150 years and provide evidence for this acceleration (Leorri et al., 2008; Rossi et al., 2011), but well-dated records over the last 300 years are lacking.

Gehrels and Woodworth (2013) re-analysed the salt-marsh RSL records referred to above, focusing on when sea-level first deviated from a background linear trend. Using only directly dated sea-level index points, they argued that the onset of modern RSL rise in the northwest Atlantic happened between AD 1925 and 1940. Inflexions around AD 1920-1930 (Woodworth, 1990) and AD 1960 have been identified in some of the longest European tide-gauge records, but these are not clear in a compilation of European records by Jevrejeva et al. (2006), perhaps reflecting the use of short record lengths in the latter analysis (Gehrels and Woodworth, 2013). There are therefore important differences in the timing and pattern of RSL change in the last several centuries in the North Atlantic that need addressing. Data archaeology is recovering some new long tide-gauge data (e.g. Haigh et al., 2009; Woodworth, 1999) but this is unlikely to generate multi-century records that are not already known. For this reason, salt-marsh archives provide an important source from which longer records can be reconstructed, especially from the northeast Atlantic coastline.

Here we develop a new 300-year sea-level reconstruction from a salt marsh on the Isle of Wight (central English Channel) that we compare with long European tide-gauge records and other salt-marsh reconstructions from the North Atlantic. We show that salt-marsh records are able to replicate the long-term sea-level rise observed by the northwest European tide-gauge records, confirming a strong spatial coherence in sea level over the last 150-300 years in this region. We obtain a long-term rate of sea-level rise since the start of the eighteenth century of 0.9 ± 0.3 mm yr^{-1}. Error-in-variables changepoint analysis does not identify statistically significant inflexions in this reconstruction. The absence of an inflexion in our Isle of Wight record differs from the pronounced inflexion observed in North American salt marsh reconstructions, particularly that from the North Carolina reported by Kemp et al. (2011). This raises some important issues, not least since the latter has been used recently as if they were a quasi-global average time series in combination with semi-empirical global models of climate-driven sea-level change (Kemp et al., 2011). The contrast emphasises the need for multiple, geographically distributed salt-marsh RSL records from across the North Atlantic to determine forcing mechanisms.

2. Study site

Newtown Estuary is located on the north side of the Isle of Wight. It is divided into six "lakes", a term derived from Old English that means "stream" or "tidal creek", that each supports extensive salt marshes and tidal flats (Figure 3). We chose to study a salt marsh on the south bank of Clamerkin Lake, to the east of Newtown village, because: i) the study area has one of the lowest tidal ranges in the English Channel (2.6 m at Spring Tide) which helps to reduce vertical uncertainties in sea-level reconstruction; ii) Newtown Estuary escaped the invasion of *Spartina alterniflora* that affected sedimentation rates in many English salt marshes in the 20th century (Hubbard and Stebbings, 1967), and iii) historic maps suggest little change in salt-marsh morphology since at least AD 1840 (the first series Ordnance Survey map), and; iv) there are several European tide gauges with long records in reasonable close proximity, notably Brest (AD 1758-present) and Newlyn (AD 1915-present) (Figure 1).

3. Methods

We collected surface sediment samples for foraminifera and organic content analyses from 2 cm vertical intervals in two transects across the marsh (Figure 4), surveying all elevations with respect to Ordnance Datum (OD) using Global Positioning System (GPS) equipment. Fossil diatoms are not preserved in the salt marsh deposits and so our sea level reconstructions are based on foraminifera and pollen that are interpreted alongside the core stratigraphies. We mapped the salt-marsh stratigraphy with seven transects (two shown here, Figure 3) using hand augers and collected sample cores from two high marsh locations (NM-6 and NM-16) using a hand-operated 8 cm-wide corer. Organic content is expressed as percentage loss on ignition (LOI) determined by combustion of material at 550^{o}C for a minimum of four hours.

We develop a chronology for our samples using Accelerator Mass Spectrometer (AMS) ^{14}C of plant macrofossils, ^{210}Pb, ^{137}Cs, ^{206}Pb/^{207}Pb, pollen markers (Figures S3 and S4) and Spherical Carbonaceous Particles (SCPs) modelled using the Bayesian age-depth BACON function in R (Blaauw and Andres Christen, 2011) (Table 1, Table S1, Figures S1 and S2). Sample preparation for measurement of ^{210}Pb, ^{137}Cs and ^{206}Pb/^{207}Pb followed standard laboratory methods, where 1 cm thick slices of fossil sediment are freeze-dried at -80^{o}C and ball-milled. ^{210}Pb and ^{137}Cs samples are then compacted into a standardised plastic gamma tubes and sealed with a rubber cap and wax. After leaving the samples undisturbed for a minimum of 21 days to allow ^{226}Ra and ^{214}Pb to achieve equilibrium the samples are placed in Ortec p-type Series Germanium gamma ray spectrometers to measure the gamma ray energies of each isotope. We relate the peak in ^{137}Cs to the peak in nuclear weapon testing in AD 1963. We construct a ‘simple’ ^{210}Pb age-depth model. Following ball milling, ^{206}Pb/^{207}Pb samples undergo microwave digestion prior to measurement of elemental concentrations by Inductively Coupled Plasma Mass Spectrometer (ICP-MS). The concentrations are then converted from ppb to ppm and reported as isotopic ratios.

Because our interest is in identifying changes in the rate of RSL change over multi-decadal to century timescales, we do not correct our records for long-term GIA which is essentially linear over these timescales. We are explicit where we compare our data with others as to whether we are comparing like-with-like or GIA-corrected rates. We calculate our rates of RSL change using weighted ordinary least squares fits, assuming a one sigma uncertainty in the vertical term and ignoring uncertainty in the age term. We also use error-in-variables Bayesian changepoint regression modelling (EIV-CP; Carlin et al., 1992; Spiegelhalter et al., 2002) to characterise the sea-level datasets in terms of rates of change and to determine the existence of inflexions ('changepoints'), if present and statistically valid. The EIV-CP approach considers both age and altitude uncertainties that are inherent characteristics of salt-marsh proxy records of sea level. We analyse three datasets using EIV-CP: the non-GIA-corrected North Carolina reconstruction (Kemp et al., 2011) and our two reconstructions from Newtown Estuary. Each dataset is analysed using five EIV-CP models in which the number of changepoints considered differs from zero to four.

4. Results

Our microfossil reconstructions are based on foraminifera and pollen. We counted 56 foraminiferal surface samples across a height range of 0.80 m from Newtown Marsh (Figure 4). The assemblage is dominated by a combination of *Jadammina macrescens* and *Trochammina inflata*, with lesser frequencies of *Quinqueloculina* sp. and *Miliamina fusca* in the low and mid marsh respectively. A low frequency assemblage of *J. macrescens* occurs above c. +1.30 m OD. The overall distribution of foraminifera is broadly comparable to that recorded on other salt marshes in the central English Channel (Horton and Edwards, 2006) (Figure S5). However, the low species diversity and turnover, and the distribution of the main taxa, notably *T. inflata* and *M. fusca* that peak in the mid marsh, mean that these data are not suitable for analysis using transfer function or matching analogue techniques due to poor model performance (r^2 <0.5) with both our local Newtown dataset (as presented in Figure 4), and when combining it with a modern British training set (Horton and Edwards, (2006) (Figure S6). Quantitative palaeoenvironmental reconstruction methods operate best with more diverse assemblages and more clearly defined optima across a range of elevations (Barlow et al., 2013; Kemp et al., 2009a; Long et al., 2010). For these reasons we focus on establishing an indicative range for each fossil sample based upon a combination of litho- and biostratigraphic information.

The lithostratigraphy comprises a pre-Holocene surface that in Transect A descends below the marsh to c. -1.50 m OD (Figure 3). An organic silt in the base of the seaward cores in Transect A is overlain by silts and clays that become increasingly organic-rich up-core. At the landward end of both transects the sediments are shallower and also become more organic. Above +0.6 m OD there is often a dark organic rich silt immediately above bedrock that is overlain by iron-stained silts that grade upwards into organic-rich silt. There is no evidence for tidal channel migration or erosion.

Each sample core was analysed for their fossil foraminifera and pollen (Figure 5). In NM-16, the higher of our sample cores, there are occasional specimens of *J. macrescens* above 54 cm that increase in abundance above 34 cm and indicate deposition in a high salt marsh. We do not place particular weight on these very low foraminiferal counts from a sea level perspective, other than to note that they suggest sedimentation between 54 cm and 34 cm occurred above the reach of normal high tides. Above 16 cm *M. fusca* appears for the first time and increases in frequency compared to the lower levels whilst those of *J. macrescens* fall. This suggests the establishment and slight lowering of the palaeomarsh surface relative to tide level, as does the occurrence of low frequencies of *Haplophragmoides wilberti* above 7 cm.

The pollen in the lower parts of NM-16 adds important information to the foraminifera data. Pollen in the base of the core (56-50 cm) indicates that a freshwater heathland developed above the pre-Holocene surface. The high frequencies of angular charcoal at this depth show that burning occurred on or close to the site, either as part of the heathland management or associated with salt making, an industry that was common in western parts of Newtown Harbour from the Medieval period onwards (Currie, 2000). The slowly-increasing up-core trend in LOI values indicate a relatively dry environment that became progressively waterlogged. This lead to the increased preservation of organic matter, likely the result of an elevation of the local freshwater table as the proximity of marine conditions to the core site increased. As tidal flooding became more common, salt marsh conditions developed. The latter is marked at 34 cm by a pronounced increase in the frequencies of halophytic pollen types, notably *Plantago maritima*, a plant that is common on high or mid marsh environments in the UK (Mossman et al., 2012), and also by low occurrences of *Armeria A* and *B* lines. The pollen data above this level suggests a slight lowering of the palaeomarsh surface with, for example, a subtle increase in frequencies of *Triglochin maritima* above 24 cm and, above 16 cm, a gradual increase in frequencies of Chenopodiaceae. The upper part of the profile is marked by an increase in tree pollen above 18 cm, notably the rise in *Pinus* and *Quercus*, which record the establishment of plantations in the region.

Loss on ignition data for core NM-16 records an increase in organic content up-core, from c. 20% at the core base to c. 45% at 8 cm, before levelling off slightly. This trend is broadly mirrored by a gradual reduction in gamma density and by an increase in the plant macrofossil content visible in the sample core. Taken together, the data described above from NM-16 record an initial phase of freshwater sedimentation above the high marsh (>+1.40 m OD between core depths 54 to 34 cm), followed by the on-site establishment of salt marsh conditions and then a slight lowering of the palaeomarsh surface from c. +1.40 m OD at 34 cm core depth to the present core top elevation of +1.32 m OD.

We analysed core NM-6 at lower resolution to assess spatial variability in RSL reconstructions from the same marsh. Core NM-6 records a broadly similar sequence to that in NM-16, although the palaeomarsh surface was lower and the rate of sedimentation higher throughout. The basal part of the core (54 to 22 cm) contains low frequencies of *J. macrescens* and *T. inflata*, indicating deposition at the highest levels of the intertidal zone. This is confirmed by low frequencies of Chenopodiaceae and *P. maritima*, together with an abundance of Poacea pollen. Above 22 cm frequencies of foraminifera increase and a mixed assemblage of *J. macrescens*, *T. inflata* and *M. fusca* is recorded and, above 16 cm, *H. wilberti*. Frequencies of *T. maritima* and then Brassicaceae pollen increase above 16 cm, confirming a lowering of the marsh surface that continues to the core top. A similar rise in *Pinus* and *Quercus* tree pollen to that observed in NM-16 occurs above 26 cm.

Age constraints for the two cores are provided by AMS ^{14}C of plant macrofossils, ^{210}Pb, ^{137}Cs, $^{206}Pb/^{207}Pb$, pollen markers and spherical carbonaceous particles (SCPs) with our most detailed dating from our main core, NM-16 (Tables 1 and S1, Figures 5 and S1). All radiocarbon dates from NM-16, except SUERC-31979 and SUERC-31991, yielded a modern age, indicating contamination by plant roots from the present surface. We do not use the modern dates in our age models. The rise in *Pinus* pollen provides a useful biostratigraphic marker in the region, dated from historical records to AD 1775 ± 25 (Long et al., 1999). SCPs in NM-16 rise above 16 cm, suggesting a date of AD 1850 ± 25 (Rose and Appleby, 2005) for this level. SCP concentrations in NM-6 were too low to count although scanning of pollen slides showed an increase above 24 cm. The ^{210}Pb profiles from both cores yield broadly linear accumulation rates and agree with peaks in ^{137}Cs (AD 1963), with an increase in metals pollution in NM-16 from the early AD 1970s attributed to discharge from the Winfrith power station (AEA, 1993; Cundy et al., 1997), and with ages inferred from stable lead isotopic ratios (Figure 5).

To develop a RSL record we compare the fossil and modern foraminifera, together with the pollen data, to define indicative meanings for samples from each core. Based on the agglutinated foraminiferal data, we are confident that the deposits in NM-16 above 34 cm, and all of those in NM-6, formed under salt marsh conditions. This is confirmed by the pollen data. The present-day salt marsh extends between +1.40 m and +0.75 m OD, which yields an initial indicative range of 1.08 ± 0.32 m. However, the reconstructions described above strongly suggest deposition occurred within a narrower vertical range located towards the upper part of the salt marsh. In particular, we note that the fossil foraminifera in both cores contain no *Quinqueloculina* sp. which in the present-day environment at Newtown Marsh (Figure 4), and elsewhere in the Solent region (Horton and

Edwards, 2006) (Figure S5), only occurs below c. +1.11 m OD. On this basis, we ascribe a narrower indicative meaning for both sediment sequences of between +1.11 m and +1.40 m OD (+1.26 ± 0.15 m), which is the highest occurrence of salt marsh at Newtown today. This is a conservative range because our pollen and microfossil data provide no evidence that either site experienced a palaeomarsh surface elevation that was ever lower than the current core top (+1.32 m OD, NM-16; +1.27 m OD, NM-6). We note that the contemporary and fossil assemblages contain few calcareous foraminifera and that this may imply some dissolution, but our reconstructions rely on the agglutinated forms and so are not affected by this.

5. Relative sea-level reconstruction

We convert our palaeomarsh surface reconstructions into RSL by using the equation:

$$\text{RSL (m)} = \text{Depth (m OD)} - \text{Reconstructed palaeomarsh surface elevation (m OD)}$$

We plot the resulting values against sample ages based on the age model for each core (Figure 6) and restrict our reconstruction in our main core (NM-16) to the last 300 years and NM-6 for the last 100 years which is the sensible limit to our age models (NM-6 has only one pre-20th century age control provided by the rise in *Pinus* pollen frequencies).

We estimate post-depositional lowering (PDL) due to compaction by applying the conceptual and numerical decompaction model developed by Brain et al. (2011; 2012) that applies a UK database of compression properties to core NM-16 (see Supplementary Information). Model results show that PDL is negligible downcore (Figure S7), peaking at 0.003 ± 0.001 m at a depth of 37 cm, and does not affect our reconstruction of sea level. The negligible PDL reflects the core stratigraphy, comprising organic, low density sediments that overly higher density sediments of lower organic content. This generates very low effective stresses (≈ 1.66 kPa at the base of the core) that cause negligible compression of sediments, which remain in their low compressibility ('over-consolidated') condition throughout.

Linear regression through the NM-16 sea-level data indicates a rate of RSL rise of 0.9 ± 0.3 mm yr^{-1} since the start of the eighteenth century (AD 1706-2011). Visual inspection of the record (Figure 6) suggests a possible acceleration in the late 19^{th} / early 20^{th} century. This coincides with a foraminiferal assemblage change that sees the replacement of a *J. macrescens* dominated assemblage by one comprising *J. macrescens* and *M. fusca*. As noted above, this indicates a slight lowering of the palaeomarsh surface relative to tide level and so this may suggest a real sea-level acceleration that occurs independently of the age-depth model. However, EIV-CP analysis shows that only the zero changepoint model converged for the NM-16 reconstruction, indicating that no statistically valid changepoints exist in this dataset. The reconstruction from NM-6 yields a RSL rise based on linear regression of 2.3 ± 1.3 mm yr^{-1} for the period since AD 1920. This compares to a rate of 1.5 ± 1.6 mm yr^{-1} over a similar period in NM-16. The higher rate of RSL from NM-6 reflects its lower position in the tidal frame which makes it less reliable for RSL reconstruction (Gehrels, 2000). Again, EIV-CP analysis indicated that the NM-6 dataset has no changepoints.

6. Discussion

6.1. Sea-level changes in the central English Channel during the last 300 years

We compare our Newtown salt-marsh RSL reconstruction with near-by tide-gauge data from Southampton and Portsmouth, based upon the recent analyses of 20^{th} century mean sea-level trends in the English Channel (uncorrected for GIA) by Haigh et al. (2009). The Southampton (AD 1935-2005) and Portsmouth (AD 1962-2007) tide gauges record rates of mean sea-level rise of 1.2 ± 0.2 mm yr^{-1} and 1.7 ± 0.3 mm yr^{-1} respectively (Figure 6). There is significant interdecadal and decadal variability in these records that can bias estimates of long-term sea-level change. Haigh et al. (2009) developed a sea-level index that represents this variability, derived from the six longest UK tide-gauge records. The index-corrected rates of Southampton and Portsmouth are 1.3 ± 0.2 mm yr^{-1} and 1.2 ± 0.3 mm yr^{-1} respectively. Both the original and index-corrected mean sea-level rates from these gauges are slightly lower than the rates inferred from our Newtown salt-marsh record (1.5 ± 1.9 and 1.5 ± 3.4 mm yr^{-1} for the respective periods for NM-16), but are consistent within the uncertainties (Figure 6).

The rate of 20th century RSL rise of 1.3 ± 1.2 mm yr^{-1} (AD 1897-2011) reconstructed from our Isle of Wight salt-marsh data is lower than the non-GIA corrected rates that are typical of the east US coast tide gauges where the effects of forebulge collapse associated with the former Laurentide Ice Sheet are significant (e.g. New York 2.7 mm yr^{-1}, Charleston 3.2 mm yr^{-1}, Halifax 3.5 mm yr^{-1} (Miller and Douglas, 2006)) (Figure 2). There are no comparably detailed salt-marsh RSL records that cover the last 300 years from elsewhere in the English Channel, but the linear rate of 0.9 ± 0.3 mm yr^{-1} since the start of the eighteenth century is consistent with that inferred over the last 2000 cal. years by Long and Tooley (1995) using late Holocene sea-level data of +1 to 1.5 mm yr^{-1}, and that inferred from historically-dated beaches in the Solent of c. +1.5 mm yr^{-1} during the last ~400 years (Nicholls and Webber, 1987) (both of the latter rates are not corrected for GIA).

6.2 Relative sea-level changes in northwest Europe during the last 300 years

The Newtown RSL record compares well with the century-scale trends recorded by the longest northwest European tide gauges (Figure 7), confirming that such records, especially if derived from a high salt-marsh setting (e.g. NM-16), can provide robust reconstructions of century-scale trends in RSL from northwest Europe. We now compare the Newtown record with the Brest tide gauge record and two other salt-marsh studies completed from northwest Europe, one from northern France (Rossi et al., 2011) and a second from northern Spain (Leorri et al., 2008) (Figure 7). We use, as a basis to aid for comparison between records, the global sea-level reconstruction based on tide-gauge data provided by Church and White (2011).

The Brest tide gauge record (Wöppelmann et al., 2008) provides a regional, long-term alternative observational record to our Newtown reconstructions and the shorter duration tide gauge records of Southampton and Portsmouth. Standard linear regression analysis for the 19th and 20th century parts of the Brest record are 0.4 ± 0.2 mm yr^{-1} and 1.1 ± 0.2 mm yr^{-1} respectively (Wöppelmann et al., 2008). In the Morbihan Gulf, Rossi et al. (2011) reconstruct a rate of RSL over the last 150 years of 1.6 ± 0.5 mm yr^{-1} that they suggest agrees with the Brest tide-gauge record but which does not replicate the long-term acceleration recorded by this tide gauge. The Spanish record from the Plentzia Estuary (Leorri et al., 2008) shows a good agreement to the linear rates of sea-level rise obtained from the tide gauge records from Santander and Brest. Their record starts in AD 1820 ± 20, chronologically tied to an increase from background levels in Pb pollution that has been dated elsewhere to AD 1800-1850 (Renberg et al., 2002). Leorri et al. (2008) propose a sea-level acceleration at c. AD 1900 but there are only three points between AD 1800 and 1920 and more data are needed to be confident in this conclusion, especially given the relatively large age and height uncertainties in the data. García-Artola et al. (2009) extend this record back to AD 1700 (see also Figure 3 in Kemp et al. (2011)) but without new dating control. We therefore do not consider this undated part of their record here.

The sites mentioned above are within 1000 km of each other on the northwest European coastline so one might expect the observed sea-level variability to be similar at each location. We can test for this by using tide-gauge and ocean-model information. For example, annual mean sea-level variability at Newlyn in Cornwall and that at Brest are almost identical throughout the 20th century, apart from a small difference in secular trend (Douglas, 2008; Haigh et al., 2009; Woodworth et al., 2009), and positive correlation exists at interannual and decadal timescales from North Sea stations to Spain (Woodworth et al., 2009; Woodworth, 1987).

We also assess spatial variability by using time series of sea level from an ocean model based on the Massachusetts Institute of Technology (MIT) general circulation model (Marshall et al., 1997a; Marshall et al., 1997b) forced by National Center for Environmental Prediction (NCEP) monthly mean wind stresses and constrained by hydrographic fields provided by the UK Meteorological Office (Smith and Murphy, 2007). This model was implemented by the University of Liverpool and National Oceanography Centre, Liverpool, and run initially for 60 years (1950–2009) at a resolution of 1/6 deg lat x 1/5 deg long. The model suggests high (zero-lag) correlation between annual mean sea-level values between southern England and Spain of approximately 0.7 (time series detrended to leave interannual and decadal signals only) or 0.8 with a 7-year filter to approximate the resolution of our salt-marsh sampling (Figure 8). A similar conclusion can be drawn from the correlation map in Figure 6 of Calafat et al. (2012) which uses a similar length time series from a different ocean model.

It is harder to assess correlation along the European coastline at longer (e.g. century) timescales using tide-gauge data, given the limitations of the available dataset. Nevertheless, the longest records from northwest Europe do suggest similar low frequency behaviour throughout the 19th and 20th centuries (Woodworth et al., 2011a), adding weight to the probability that the Atlantic coast might display similar century-timescale changes. Model runs of an Atmosphere-Ocean General Circulation Model (HadCM3) that uses anthropogenic climate forcings (the ALL250 run of Gregory et al. (2006)) gives essentially complete coherence of sea level along the European coastline (correlation coefficient of 0.95 using all annual mean values from detrended time series from southern England and northern Spain, and 0.98 with a 7 year filter applied to both series). However, given the limited spatial resolution of such AOGCMs, we are cautious regarding model ability to resolve the narrow shelves in the southern part of the coastline and thereby to represent its sea-level response to the local ocean dynamics.

6.3 Relative sea-level changes in the North Atlantic during the last 300 years

A defining feature of the late Holocene RSL record from several salt marshes in the northwest Atlantic is an abrupt acceleration (or inflexion) in the late 19th or early 20th century that is observed against a long-term upwards trend in RSL caused by long term glacio-isostatic subsidence due largely to the collapse of the Laurentide Ice Sheet forebulge. This is different to the records described above from the northeast Atlantic. Although RSL trends along each basin margin are broadly similar, the overall rise in RSL is larger in the west and the biggest contributor to these differences is the late 19th / early 20th century sea-level acceleration (Figure 7). The reconstruction from North Carolina by Kemp et al. (2011) is the best dated and most precise sea-level reconstruction from the North Atlantic, and has been used by these authors to infer climate-sea-level forcing during the last 1000 years or so. The site has a low tidal range that helps keep vertical errors of the reconstruction small, and excellent dating control developed using a range of methods similar to those applied to the Newtown sequence. The acceleration reported by Kemp et al. (2011) in North Carolina between AD 1865 and AD 1892 saw the rate of detrended (GIA corrected) sea-level increase from -0.1 mm yr^{-1} to +2.1 mm yr^{-1}, a change of +2.2 mm yr^{-1}. Our new record from Newtown does not record such an acceleration on the basis of the same analytical technique (EIV-CP). Similarly, simple linear regression change point analysis (Carlin et al., 1992) does not identify a synchronous acceleration in the Brest tide gauge record (data not shown). The different manifestation of this acceleration across the Atlantic cannot be explained by glacio-isostasy, which is essentially linear over these timescales, and implicates other, regionally-specific processes.

There are good reasons to expect contrasts in sea-level change across the North Atlantic, given the region's complex and linked atmospheric and oceanographic circulation. For example, variations in air-pressure and wind stress resulting in spin-up/down of the North Atlantic sub-tropical gyre (Miller and Douglas, 2007; Woodworth et al., 2010) or as changes in longshore wind forcing (Sturges and Douglas, 2011; Sturges and Hong, 1995) have been suggested as correlating with multi-decadal changes in coastal sea-level observed by North Atlantic tide gauges on both ocean margins. As sea-level pressure increases (decreases) at the centre of the subtropical atmospheric gyre, the atmospheric gyre spins up (down) and water is re-distributed such that the rate of sea-level rise along the eastern margin of the North Atlantic falls (rises) (Miller and Douglas, 2007). If ocean gyres change in strengths on centennial timescales, which has not yet been established, then this re-distribution mechanism provides one hypothesis for the faster 20th century sea-level rise in the western Atlantic.

Dynamic processes are in addition to any spatially variable signal, or "sea-level fingerprint" associated with mass exchange between the land-based ice and the oceans. Such mass changes provide a second hypothesis to explain the contrasts we observe in RSL across the North Atlantic. The exact pattern of any mass-driven sea-level fingerprint depends on the source of the mass change. Sea-level fingerprints from a uniform Greenland melt create small, mainly north-south sea-level gradients across the North Atlantic, with the UK located on the zero-isobase contour and north to south gradients along the northeast coast of the USA of c. 0.6 mm between Newfoundland and Cape Hatteras (Mitrovica et al., 2001). Uniform melt of Antarctica and mountain glaciers generate no significant sea-level gradients across the North Atlantic (Mitrovica et al., 2001). However, more spatially complex melt histories do have the potential to create spatially complex sea-level finger-prints in the North Atlantic. West Antarctic focused melt generates several "hot spots" of sea-level rise, one of which is centred on the north and central east coast of North America where rates of sea-level rise are predicted to be 25-30% higher than the global average (Mitrovica et al., 2009). Melt from Arctic and Alaskan glaciers can also produce east-west gradients across the North Atlantic Ocean (Bamber and Riva, 2010), but observational records supporting spatially variable melt histories are limited in their duration and resolution. Records from the Arctic glaciers suggest that these only reached their maxima in the 1920s and 1930s; 19th century regional observations are not available (Marzeion et al., 2012). Century-scale melt histories from different parts of Antarctica are also currently lacking (e.g. Nakada et al., 2013). Greenland has one of the longest melt histories but it seems unlikely that any late 19th century acceleration contains a significant Greenland component, with modelling by Box and Colgan (2013) suggesting a zero contribution from this source (0.0 mm yr^{-1} sea-level equivalent between AD 1845-1893), compared to the 2.2 mm yr^{-1} detrended (GIA corrected) acceleration proposed in North Carolina at this time (Kemp et al., 2011). Moreover, any modest Greenland contribution, or indeed that from other land-based ice sources, would potentially be overprinted by dynamic sea-level variability caused by atmospheric and oceanographic processes; Kopp et al. (2010) show that with a theoretical network of 150 tide gauges, a 0.2 mm yr^{-1} equivalent sea-level melt from Greenland would only be detectable above the dynamic sea-level variability after 50 years of observation (95% confidence).

Interestingly, Kopp et al. (2010) also show that the east US coast is sensitive to changes in the speed of the Atlantic meridional overturning circulation (AMOC), citing the model predictions of Bingham and Hughes (2009) that predict a 2 cm rise in sea-level for every 1 Sv slow-down in AMOC. This mechanism provides a third hypothesis to explain the faster rates of sea-level rise in the north-west Atlantic. Indeed, slowdown of AMOC is suggested by Sallenger et al. (2012) as an explanation for rapid rates of sea-level rise along the North American east coast between AD 1950-1979 and AD 1980-2009, although Kopp (2013) shows that this 'hot spot' anomaly is within the range of past variability and is correlated with Atlantic Multidecadal Oscillation, North Atlantic Oscillation and Gulf Stream North Wall indices. Were changes in the AMOC the main driver of the North Carolina sea-level acceleration of ~2 mm yr^{-1} it would require a sustained AMOC slow-down starting in the late 19th / early 20th century. Well-dated records of AMOC speed are limited, but Lund et al. (2006) show that for the Florida Current, which is one component of the North Atlantic circulation, the opposite occurred with a sustained acceleration in the current after the end of the Little Ice Age (dated to c. AD 1800).

Much of this discussion is based on the assumption that the salt-marsh reconstructions from the east USA coast faithfully capture the timing and magnitude of the late 19th / early 20th century sea-level acceleration. However, the US east coast lacks copious and continuous tide-gauge data spanning this key time interval (Figure 2). There is only one gauge that spans the period of interest (New York (The Battery), AD 1856-present)) which exhibits an acceleration of approximately 0.008 mm yr^{-2} which is less than that found at European sites (Woodworth et al., 2011b). Moreover, it does not record the strong acceleration seen in the North Carolina salt-marsh study between AD 1865-1892 (Kemp et al., 2011). Notwithstanding this, the New York record has been compared with proxy data from a Connecticut salt marsh (Donnelly et al., 2004) to argue for a sharp acceleration between AD 1850 and 1900. However, the proxy reconstruction in this study was based on low-resolution basal peats and did not significantly overlap with the instrumental data. Moreover, Gehrels and Woodworth (2013) suggest that the Connecticut record starts departing from the millennial-scale late Holocene background trend between AD 1920 and 1930 and the North Carolina record between AD 1925 and 1935.

In summary, RSL records from both sides of the North Atlantic do not record a synchronous acceleration in RSL during the late 19th / early 20th century (Figure 7). Whilst variations in timing and rate can be due to dating resolution and uncertainties, the variability is important. The acceleration in the North Carolina record is much faster and larger than that seen in other salt-marsh records and tide gauges from North America and northwest Europe. Indeed, mindful that this is a subsiding coast on late Holocene timescales, the presence of such a strong sea-level acceleration signal is all the more notable.

These differences are of interest because reliable, long sea-level records that span several centuries or more are being used as if they were quasi-global within semi-empirical model parameterisations that seek to predict future sea-level rise using global average temperatures. Presently the North

Carolina RSL curve is the only such proxy sea-level record used by these models (Kemp et al., 2011; Rahmstorf et al., 2012; Schaeffer et al., 2012), and predicts a 'global' sea-level rise of ~ 1 m for a 1.8°C warming by AD 2100. Its usage is justified on the basis that the GIA corrected record is thought to be a reliable measure of global sea-level change (within ± 0.10 cm, equal to more than half the 0.24 m 20th century sea-level rise at this site) (Kemp et al., 2011). Our study suggests that the RSL records from the northeast and northwest Atlantic differ to that from North Carolina, particularly with regard to the magnitude of the sea-level changes during the late 19th and early 20th century. We propose that this part of the North Carolina record records a regionally specific amplification of more muted changes observed elsewhere in the North Atlantic. The cause of this difference is not obvious but three potential hypotheses are that it records changes in the spin-up/down of the North Atlantic sub-tropical gyre, changes in land-based ice mass, or variations in AMOC strength. Moreover, these regional-scale differences highlight the value of using several, regionally representative RSL records when calibrating and testing semi-empirical models of sea-level against palaeo-records. When using records that over-estimate sea-level rise in the past the models will also over-estimate sea-level rise in the future.

6. Conclusions

A defining feature of most tide-gauge records that contain over ~100 years of data is a gradual acceleration in sea-level that is dated to the late 19th / early 20th century. In the northwest Atlantic, only one such gauge exists (New York (The Battery)) and this is incomplete across this interval, yet several salt-marsh sea-level reconstructions from the region record a pronounced RSL acceleration at this time. The most detailed of these is from North Carolina, where detrended (GIA corrected) sea-level accelerated by c. 2.2 mm yr^{-1} between AD 1865-1892 (Kemp et al., 2011). This record is important since it has been used to identify strong climate-sea-level forcing at this time and to calibrate a semi-empirical model of global climate and sea-level (e.g. Kemp et al., 2011; Rahmstorf et al., 2012).

Prior to this study there were only two salt marsh-based RSL reconstructions from the northeast Atlantic margin. Here we develop a longer and more precise record, from Newtown marsh (Isle of Wight), that we compare with other RSL records from both sides of the North Atlantic. Our key conclusions are:

1. The rate of RSL rise for the whole record (not GIA corrected) from our best-dated core (NM-16) is 0.9 ± 0.3 mm yr^{-1} since the start of the eighteenth century (AD 1706-2011). Error-in-variables changepoints analysis does not identify a statistically significant inflexion in the rate of sea-level rise within this record.
2. The Newtown record broadly agrees with trends recorded by tide gauges and two other salt-marsh records from the northwest European coastline, confirming that salt-marsh records derived from a high marsh setting can provide robust reconstructions of century-scale trends in RSL from this region.
3. Compared to the northwest Atlantic salt-marsh records, a late 19th / early 20th century sea-level acceleration is muted or absent in the northeast Atlantic. In particular, the abrupt acceleration in late 19th century RSL recorded in North Carolina by Kemp et al. (2011) appears to record a locally-amplified sea-level signal. Demonstrating this regional variation in North Atlantic sea-level change is important as it shows that no single site is representative of ocean-wide trends.

Acknowledgements

Funding for this work was provided by UK Natural Environment Research Council grant “North Atlantic sea-level change and climate in the last 500 years” (NE/G004757/1). Radiocarbon dating support comes from the Natural Environment Research Council Radiocarbon Committee, allocation #1490.0810. Professor Ric Williams and Dr Vassil Roussenov, Liverpool University are thanked for their help with the Liverpool/MIT ocean model. We also thank Rob Barnett, Lucy Goodman, Marta Perez Fernandez and David Tomlinson for their assistance in the field and Martin West and Amanda Hayton in the Geography Department at Durham University for preparation and analysis of the gamma and ICP-MS samples. We are grateful to Andrew Parnell (University College Dublin) for helpful discussions regarding change-point modelling. The National Trust and Natural England provided access to the Newtown salt marsh. We thank reviewers and the Editor, Professor Gideon Henderson, for helpful and constructive comments. This paper has benefited from discussions with members of PALSEA (a PAGES/INQUA/WUN working group) and is a contribution to that programme and to the INQUA Commission on Coastal and Marine Processes and to IGCP 588 "Preparing for coastal change: A detailed process-response framework for coastal change at different timescales".

References

AEA, 1993. Annual report on radioactive discharges from Winfrith and monitoring the environment 1992.

Bamber, J., Riva, R., 2010. The sea level fingerprint of recent ice mass fluxes. The Cryosphere 4, 621-627.

Barlow, N.L.M., Shennan, I., Long, A.J., Gehrels, W.R., Saher, M.H., Woodroffe, S.A., Hillier, C., 2013. Salt marshes as geological tide gauges. Global and Planetary Change 106, 90-110.

Bingham, R.J., Hughes, C.W., 2009. Signature of the Atlantic meridional overturning circulation in sea level along the east coast of North America. Geophysical Research Letters 36.

Blaauw, M., Andres Christen, J., 2011. Flexible Paleoclimate Age-Depth Models Using an Autoregressive Gamma Process. Bayesian Analysis 6, 457-474.

Box, J.E., Colgan, W., 2013. Greenland Ice Sheet Mass Balance Reconstruction. Part III: Marine Ice Loss and Total Mass Balance (1840–2010). Journal of Climate 26, 6990-7002.

Brain, M.J., Long, A.J., Petley, D.N., Horton, B.P., Allison, R.J., 2011. Compression behaviour of minerogenic low energy intertidal sediments. Sedimentary Geology 233, 28-41.

Brain, M.J., Long, A.J., Woodroffe, S.A., Petley, D.N., Milledge, D.G., Parnell, A.C., 2012. Modelling the effects of sediment compaction on salt marsh reconstructions of recent sea-level rise. Earth and Planetary Science Letters 345, 180-193.

Calafat, F.M., Chambers, D.P., Tsimplis, M.N., 2012. Mechanisms of decadal sea level variability in the eastern North Atlantic and the Mediterranean Sea. Journal of Geophysical Research: Oceans 117, C09022.

Carlin, B.P., Gelfand, A.E., Smith, A.F.M., 1992. Hierarchical Bayesian Analysis of Changepoint Problems. Journal of the Royal Statistical Society. Series C (Applied Statistics) 41, 389-405.

Church, J.A., White, N.J., 2011. Sea-Level Rise from the Late 19th to the Early 21st Century. Surveys in Geophysics 32, 585-602.

Cundy, A.B., Croudace, I.W., Thomson, J., Lewis, J.T., 1997. Reliability of salt marshes as "geochemical recorders" of pollution input : a case study from contrasting estuaries in southern England. Environmental Science and Technology 31, 1093-1101.

Currie, C.K., 2000. An archaeological and historical survey of the Newtown Estate, Newtown, Isle of Wight. Centred on SZ 424906. , Report to the National Trust (Southern Region), CKC Archaeology.

Donnelly, J.P., Cleary, P., Newby, P., Ettinger, R., 2004. Coupling instrumental and geological records of sea-level change: Evidence from southern New England of an increase in the rate of sea-level rise in the late 19th century. Geophysical Research Letters 31.

Douglas, B.C., 2008. Concerning evidence for fingerprints of glacial melting. Journal of Coastal Research 24, 218-227.

García-Artola, A., Cearreta, A., Leorri, E., Irabien, M.J., Blake, W.H., 2009. Las marismas costeras como archivos geológicos de las variaciones recientes en el nivel marino. Geogaceta 47, 109-112.

Gehrels, W.R., 2000. Using foraminiferal transfer functions to produce high-resloution sea-level records from salt-marsh deposits, Maine, USA. The Holocene 10, 367-376.

Gehrels, W.R., Kirby, J.R., Prokoph, A., Newnham, R.M., Achterberg, E.P., Evans, H., Black, S., Scott, D.B., 2005. Onset of recent rapid sea-level rise in the western Atlantic Ocean. Quaternary Science Reviews 24, 2083.

Gehrels, W.R., Woodworth, P.L., 2013. When did modern rates of sea-level rise start? Global and Planetary Change 100, 263-277.

Gregory, J.M., Lowe, J.A., Tett, S.F.B., 2006. Simulated global-mean sea level changes over the last half-millennium. Journal of Climate 19, 4576-4591.

Grenfell, H.R., Hayward, B.W., Nomura, R., Sabaa, A.T., 2012. A foraminiferal proxy record of 20th century sea-level rise in the Manukau Harbour, New Zealand. Marine and Freshwater Research 63, 370-384.

Haigh, I., Nicholls, R., Wells, N., 2009. Mean sea level trends around the English Channel over the 20th century and their wider context. Cont. Shelf Res. 29, 2083-2098.

Horton, B.P., Edwards, R.J., 2006. Quantifying Holocene sea-level change using intertidal foraminifera: Lessons from the British Isles. Cushman Foundation for Foraminiferal Research Special Publication, 3-97.

Hubbard, J.C.E., Stebbings, R.E., 1967. Distribution, date of origin and acreage of Spartina townsendii (s.l.) marshes in Great Britain. Proceedings of the Botanical Society of the British Isles 1, 1-7.

Jevrejeva, S., Grinsted, A., Moore, J.C., Holgate, S., 2006. Nonlinear trends and multiyear cycles in sea level records. Journal of Geophysical Research-Oceans 111.

Kemp, A.C., Horton, B.P., Culver, S.J., 2009a. Distribution of modern salt-marsh foraminifera in the Albemarle-Pamlico estuarine system of North Carolina, USA: Implications for sea-level research. Marine Micropaleontology 72, 222-238.

Kemp, A.C., Horton, B.P., Culver, S.J., Corbett, D.R., van de Plassche, O., Gehrels, W.R., Douglas, B.C., Parnell, A.C., 2009b. Timing and magnitude of recent accelerated sea-level rise (North Carolina, United States). Geology 37, 1035-1038.

Kemp, A.C., Horton, B.P., Donnelly, J.P., Mann, M.E., Vermeer, M., Rahmstorf, S., 2011. Climate related sea-level variations over the past two millennia. Proceedings of the National Academy of Sciences of the United States of America 108, 11017-11022.

Kopp, R.E., 2013. Does the mid-Atlantic United States sea level acceleration hot spot reflect ocean dynamic variability? Geophysical Research Letters 40, 3981-3985.

Kopp, R.E., Mitrovica, J.X., Griffies, S.M., Yin, J., Hay, C.C., Stouffer, R.J., 2010. The impact of Greenland melt on local sea levels: a partially coupled analysis of dynamic and static equilibrium effects in idealized water-hosing experiments. Climatic change 103, 619-625.

Leorri, E., Horton, B.P., Cearreta, A., 2008. Development of a foraminifera-based transfer function in the Basque marshes, N. Spain: Implications for sea-level studies in the Bay of Biscay. Marine Geology 251, 60-74.

Long, A.J., Scaife, R.G., Edwards, R.J., 1999. Pine pollen in intertidal sediments from Poole Harbour, UK; implications for late-Holocene sediment accretion rates and sea-level rise. Quaternary International 55, 3-16.

Long, A.J., Tooley, M.J., 1995. Holocene sea-level and crustal movements in Hampshire and southeast England, United Kingdom. Journal of Coastal Research 17, 299-310.

Long, A.J., Woodroffe, S.A., Milne, G.A., Bryant, C.L., Wake, L.M., 2010. Relative sea level change in west Greenland during the last millennium. Quaternary Science Reviews 29, 367-383.

Lund, D.C., Lynch-Stieglitz, J., Curry, W.B., 2006. Gulf Stream density structure and transport during the past millennium. Nature 444, 601-604.

Marshall, J., Adcroft, A., Hill, C., Perelman, L., C., H., 1997a. A finite volume,incompressible Navier-Stokes model for studies ocean on parallel computers. Journal of Geophysical Research 102, 5753–5766.

Marshall, J., Hill, C., Perelman, L., Adcroft, A., 1997b. Hydrostatic, quasi-hydrostatic, and nonhydrostatic ocean modelling. Journal of Geophysical Research 102, 5733–5752.

Marzeion, B., Jarosch, A.H., Hofer, M., 2012. Past and future sea-level change from the surface mass balance of glaciers. The Cryosphere 6, 1295-1322.

Miller, L., Douglas, B.C., 2006. On the rate and causes of twentieth century sea-level rise. Philosophical Transactions of the Royal Society a-Mathematical Physical and Engineering Sciences 364, 805-820.

Miller, L., Douglas, B.C., 2007. Gyre-scale atmospheric pressure variations and their relation to 19th and 20th century sea level rise. Geophysical Research Letters 34.

Mitrovica, J.X., Gomez, N., Clark, P.U., 2009. The Sea-Level Fingerprint of West Antarctic Collapse. Science 323, 753.

Mitrovica, J.X., Tamisiea, M.E., Davis, J.L., Milne, G.A., 2001. Recent Mass Balance of Polar Ice Sheets Inferred From Patterns of Global Sea-Level Change,. Nature 409, 1026-1029.

Mossman, H.L., Davy, A.J., Grant, A., 2012. Does managed coastal realignment create saltmarshes with ‘equivalent biological characteristics’ to natural reference sites? Journal of Applied Ecology 49, 1446-1456.
Nakada, M., Okuno, J.i., Ishii, M., 2013. Twentieth century sea-level rise inferred from tide gauge, geologically derived and thermosteric sea-level changes. Quaternary Science Reviews 75, 114-131.
Nicholls, R.J., Webber, N.B., 1987. The past, present and future evolution of Hurst-Castle-Spit, Hampshire. Progress in Oceanography 18, 119-137.
Rahmstorf, S., Foster, G., Cazenave, A., 2012. Comparing climate projections to observations up to 2011. Environ. Res. Lett. 7.
Renberg, I., Brannvall, M.L., Bindler, R., Emteryd, O., 2002. Stable lead isotopes and lake sediments - a useful combination for the study of atmospheric lead pollution history. Science of the Total Environment 292, 45-54.
Rose, N.L., Appleby, P.G., 2005. Regional applications of lake sediment dating by spheroidal carbonaceous particle analysis I: United Kingdom. Journal of Paleolimnology 34, 349-361.
Rossi, V., Horton, B.P., Corbett, D.R., Leorri, E., Perez-Belmonte, L., Douglas, B.C., 2011. The application of foraminifera to reconstruct the rate of 20th century sea level rise, Morbihan Golfe, Brittany, France. Quaternary Research 75, 24-35.
Sallenger, A.H., Jr., Doran, K.S., Howd, P.A., 2012. Hotspot of accelerated sea-level rise on the Atlantic coast of North America. Nature Climate Change 2, 884-888.
Schaeffer, M., Hare, W., Rahmstorf, S., Vermeer, M., 2012. Long-term sea-level rise implied by 1.5[thinsp][deg]C and 2[thinsp][deg]C warming levels. Nature Clim. Change 2, 867-870.
Smith, D.M., Murphy, J.M., 2007. An objective ocean temperature and salinity analysis using covariances from a global climate model. Journal of Geophysical Research 112, C02022.
Spiegelhalter, D.J., Best, N.G., Carlin, B.P., Van Der Linde, A., 2002. Bayesian measures of model complexity and fit. Journal of the Royal Statistical Society: Series B (Statistical Methodology) 64, 583-639.
Sturges, W., Douglas, B.C., 2011. Wind effects on estimates of sea level rise. Journal of Geophysical Research-Oceans 116.
Sturges, W., Hong, B.G., 1995. Wind forcing of the Atlantic thermocline along 32-degrees-N at low frequencies. Journal of Physical Oceanography 25, 1706-1715.
van de Plassche, O., 2000. North Atlantic climate-ocean variations and sea level in Long Island sound, Connecticut, since 500 cal yr AD. Quaternary Research 53, 89-97.
Woodworth, P., Menéndez, M., Gehrels, W., 2011a. Evidence for century-timescale acceleration in mean sea levels and for recent changes in extreme sea levels. Surveys in Geophysics 32, 603-618.
Woodworth, P., Teferle, F., Bingley, R., Shennan, I., Williams, S., 2009. Trends in UK mean sea level revisited. Geophysical Journal International 176, 19-30.
Woodworth, P.L., 1987. Trends in UK mean sea level. Marine Geodesy 11, 57-87.
Woodworth, P.L., 1990. A search for accelerations in records of European mean sea level. Int. J. Climatol. 10, 129-143.
Woodworth, P.L., 1999. High waters at Liverpool since 1768: the UK's longest sea level record. Geophysical Research Letters 26, 1589-1592.
Woodworth, P.L., Gehrels, W.R., Nerem, R.S., 2011b. Nineteenth and twentieth century changes in sea level. Oceanography 24, 80-93.
Woodworth, P.L., Pouvreau, N., Woeppelmann, G., 2010. The gyre-scale circulation of the North Atlantic and sea level at Brest. Ocean Science 6, 185-190.
Wöppelmann, G., Pouvreau, N., Coulomb, A., Simon, B., Woodworth, P.L., 2008. Tide gauge datum continuity at Brest since 1711: France's longest sea-level record. Geophysical Research Letters 35.

Figure captions

Figure 1 Location map showing key tide-gauge and salt-marsh study sites mentioned in the text. The approximate configuration of the Gulf Stream and direction of the ocean gyres is shown for illustrative purposes.

Figure 2 Selected tide-gauge records from the North Atlantic. Data are sourced from the Permanent Service for Mean Sea-level (http://www.psmsl.org/), with the Southampton record by Haigh et al. (2009). The salt-marsh RSL reconstruction of Kemp et al. (2011) from North Carolina is also shown. None of the records are corrected for vertical land motions (GIA). The vertical shaded bar denotes the period of sea-level acceleration identified in North Carolina salt-marsh sediments by Kemp et al. (2011).

Figure 3 The study site showing: (A) the Isle of Wight, (B) Newtown Estuary, (C) Newtown Marsh with contemporary sampling and stratigraphic survey transects, (D) simplified lithostratigraphy of the two stratigraphic survey transects.

Figure 4 Modern vertical distribution of foraminifera across the Newtown Marsh. The shaded bar on the left hand of the diagram is the range of the indicative meanings used to reconstruct RSL from the fossil foraminfera.

Figure 5 Lithology, biostratigraphy and chronology from NM-16 and NM-6. The lithostratratigraphic symbols are as in Figure 3. Full pollen data are available in supplementary information.

Figure 6 Newtown relative sea-level reconstructions: reconstruction from NM-16 (dark grey) and NM-6 (light grey) compared with tide-gauge data from Brest (blue), Portsmouth (yellow) and Southampton (red) (data are smoothed using a 7-year moving average, and are sourced from the Permanent Service for Mean Sea-level (http://www.psmsl.org/). The width of the boxes in (A) equals the 2 sigma age range of each sample and the box height the indicative range as detailed in the text. None of the data are corrected for vertical land motions.

Figure 7 A comparison of sea-level records from the west and east Atlantic during the last 300 years. Tide-gauge data in (B) and (F) are sourced from the Permanent Service for Mean Sea-level (http://www.psmsl.org/) and are smoothed with a seven year moving average to approximate the sampling resolution of the salt-marsh data. The colours correspond to the tide gauge location markers on the map. Salt marsh relative sea-level reconstructions are from: Chezzetcook (Gehrels et al., 2005), Barn Island, Connecticut (Donnelly et al., 2004), North Carolina (Kemp et al., 2011), Newtown, Isle of Wight (this study), Morbihan Gulf (Rossi et al., 2011) and Plentizia Estuary (Leorri et al. 2009). All data series are plotted against the Church and White (2011) global mean sea level reconstruction (in red) for ease of comparison between datasets.

Figure 8 Correlation coefficients in time series of annual mean sea level between a point in southern England (Newlyn) and each point in the grid of an ocean model developed by Liverpool University based on the Massachusetts Institute of Technology (MIT) general circulation model. Time series span the period 1950-2009 and have been low-pass filtered with a 7-year filter to approximate the resolution of marsh sampling.

Table 1 Dating control for the Newtown Marsh sample cores.

Depth (cm)	^{14}C yr BP (± 1σ)	Age (yr AD)	Error	Chronological control
NM-16				
0.0	-	2010.0	0.5	Core top
0.5 ± 0.5	-	2004.3	0.4	^{210}Pb simple age model
1.5 ± 0.5	-	1998.0	0.9	^{210}Pb simple age model
2.5 ± 0.5	-	1990.4	1.5	^{210}Pb simple age model
3.5 ± 0.5	-	1982.5	2.2	^{210}Pb simple age model
4.5 ± 0.5	-	1980.0	5.0	Increase in ^{206}Pb/^{207}Pb
4.5 ± 0.5	-	1976.6	2.6	^{210}Pb simple age model
4.5 ± 0.5	-	1975.0	5.0	Winfrith pollutant increase
5.5 ± 0.5	-	1971.7	3.0	^{210}Pb simple age model
6.5 ± 0.5	-	1966.8	3.4	^{210}Pb simple age model
7.5 ± 0.5	-	1963.0	5.0	^{137}Cs peak
7.5 ± 0.5	-	1961.7	3.8	^{210}Pb simple age model
8.5 ± 0.5	-	1955.5	4.3	^{210}Pb simple age model
9.5 ± 0.5	-	1947.6	4.9	^{210}Pb simple age model
10.5 ± 0.5	-	1940.2	5.5	^{210}Pb simple age model
11.5 ± 0.5	-	1927.7	6.5	^{210}Pb simple age model
12.5 ± 0.5	-	1915.1	7.5	^{210}Pb simple age model
13.5 ± 0.5	-	1902.6	8.5	^{210}Pb simple age model
14.0 ± 2.0	-	1850.0	25.0	Onset of SCP's
14.5 ± 0.5	-	1890.3	9.4	^{210}Pb simple age model
16.5 ± 0.5		1825.0	25.0	Decrease in ^{206}Pb/^{207}Pb
16.5 ± 0.5	-	1820.0	20.0	Rise in total lead
22.0 ± 2.0	-	1775.0	25.0	Rise in pine pollen frequencies
29.5 ± 0.5	105.0 ± 17	1806.5*	111.5	Radiocarbon date on unidentified plant macrofossil (SUERC-31979)
29.5 ± 0.5	105.0 ± 16	1806.5*	111.5	Radiocarbon date on unidentified plant macrofossil (SUERC-31991)
NM-6				
0.0	-	2009.0	0.5	Core top
1.5 ± 0.5	-	2005.6	0.4	^{210}Pb simple age model
2.5 ± 0.5	-	2001.5	0.8	^{210}Pb simple age model
3.5 ± 0.5	-	1996.7	1.4	^{210}Pb simple age model
4.5 ± 0.5	-	1991.9	1.9	^{210}Pb simple age model
5.5 ± 0.5	-	1987.3	2.4	^{210}Pb simple age model
6.5 ± 0.5	-	1983.4	2.8	^{210}Pb simple age model
7.5 ± 0.5	-	1979.2	3.3	^{210}Pb simple age model
8.5 ± 0.5	-	1975.6	3.7	^{210}Pb simple age model
9.5 ± 0.5	-	1972.1	4.1	^{210}Pb simple age model
10.5 ± 0.5	-	1968.2	4.5	^{210}Pb simple age model
11.5 ± 0.5	-	1963.0	5.0	^{137}Cs peak
11.5 ± 0.5	-	1964.0	5.0	^{210}Pb simple age model
12.5 ± 0.5	-	1958.7	5.6	^{210}Pb simple age model
13.5 ± 0.5	-	1954.3	6.0	^{210}Pb simple age model
14.5 ± 0.5	-	1950.0	6.5	^{210}Pb simple age model
15.5 ± 0.5	-	1946.0	7.0	^{210}Pb simple age model

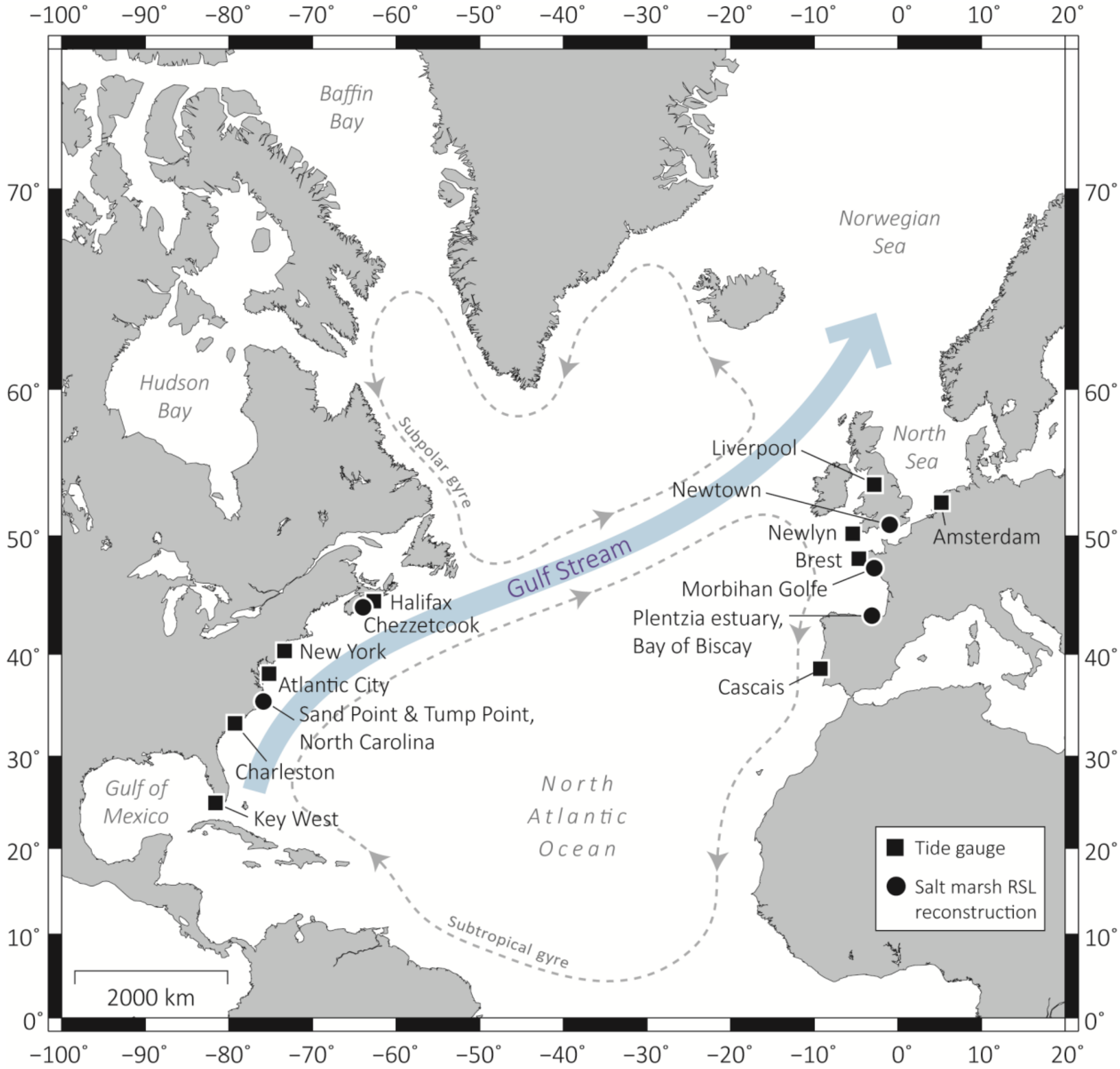

Baffin Bay
Hudson Bay
Norwegian Sea
North Sea
Subpolar gyre
Gulf Stream
Liverpool
Newtown
Newlyn
Brest
Amsterdam
Morbihan Golfe
Plentzia estuary, Bay of Biscay
Cascais
Halifax
Chezzetcook
New York
Atlantic City
Sand Point & Tump Point, North Carolina
Charleston
Key West
Gulf of Mexico
North Atlantic Ocean
Subtropical gyre
Tide gauge
Salt marsh RSL reconstruction
2000 km

Figure 1

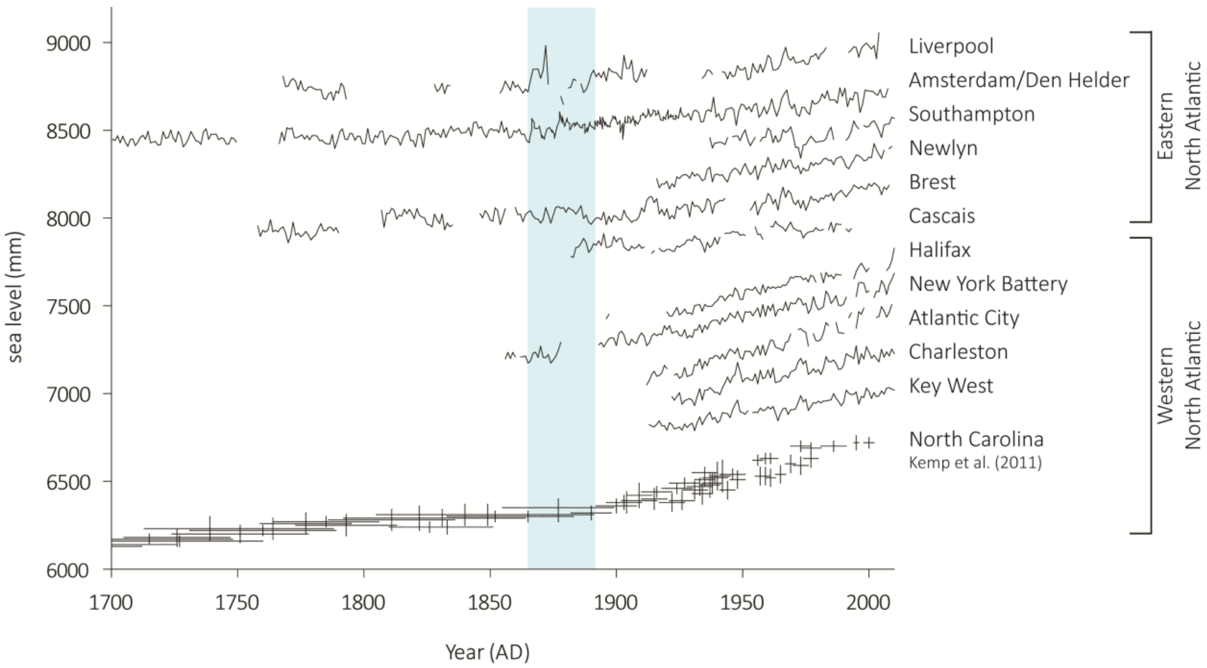

Liverpool
Amsterdam/Den Helder
Southampton
Newlyn
Brest
Cascais
Halifax
New York Battery
Atlantic City
Charleston
Key West
North Carolina
Kemp et al. (2011)
Eastern North Atlantic
Western North Atlantic
sea level (mm)
Year (AD)
9000
8500
8000
7500
7000
6500
6000
1700
1750
1800
1850
1900
1950
2000

Figure 2

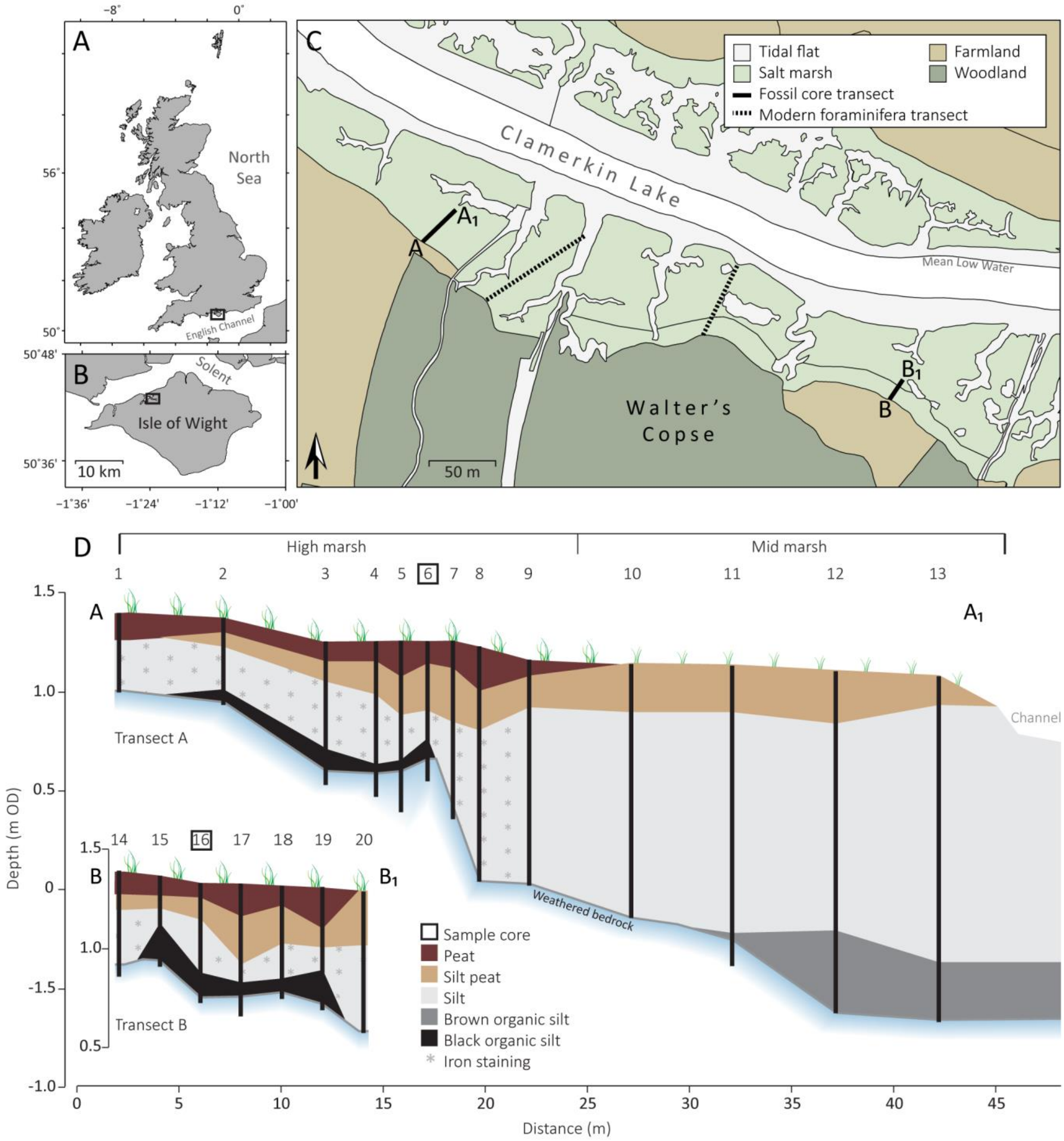

A
North Sea
English Channel
B
Solent
Isle of Wight
10 km
C
Tidal flat
Salt marsh
Farmland
Woodland
Fossil core transect
Modern foraminifera transect
Clamerkin Lake
Mean Low Water
Walter's Copse
50 m
D
High marsh
Mid marsh
Transect A
Transect B
Channel
Weathered bedrock
Sample core
Peat
Silt peat
Silt
Brown organic silt
Black organic silt
Iron staining
Depth (m OD)
Distance (m)

Figure 3

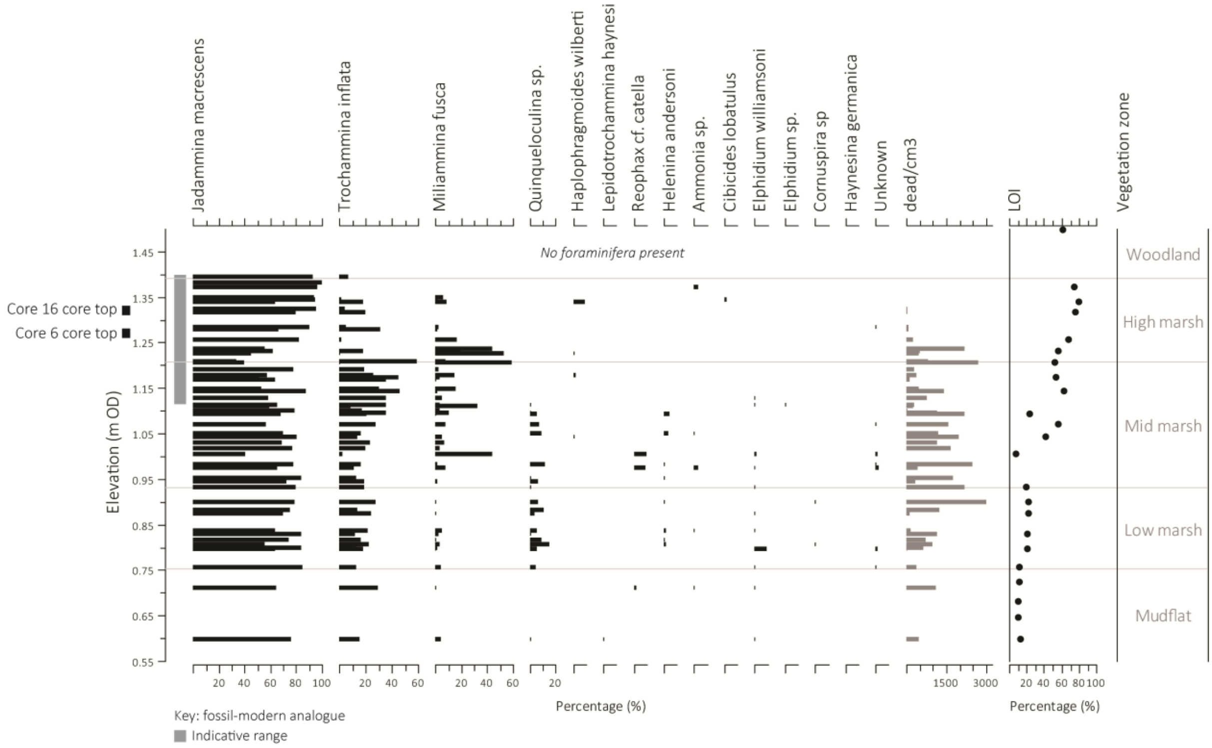
Jadammina macrescens
Trochammina inflata
Miliammina fusca
Quinqueloculina sp.
Haplophragmoides wilberti
Lepidotrochammina haynesi
Reophax cf. catella
Helenina andersoni
Ammonia sp.
Cibicides lobatulus
Elphidium williamsoni
Elphidium sp.
Cornuspira sp
Haynesina germanica
Unknown
dead/cm3
LOI
Vegetation zone
No foraminifera present
Woodland
High marsh
Mid marsh
Low marsh
Mudflat
Core 16 core top
Core 6 core top
Elevation (m OD)
Percentage (%)
Percentage (%)
Key: fossil-modern analogue
Indicative range

Figure 4

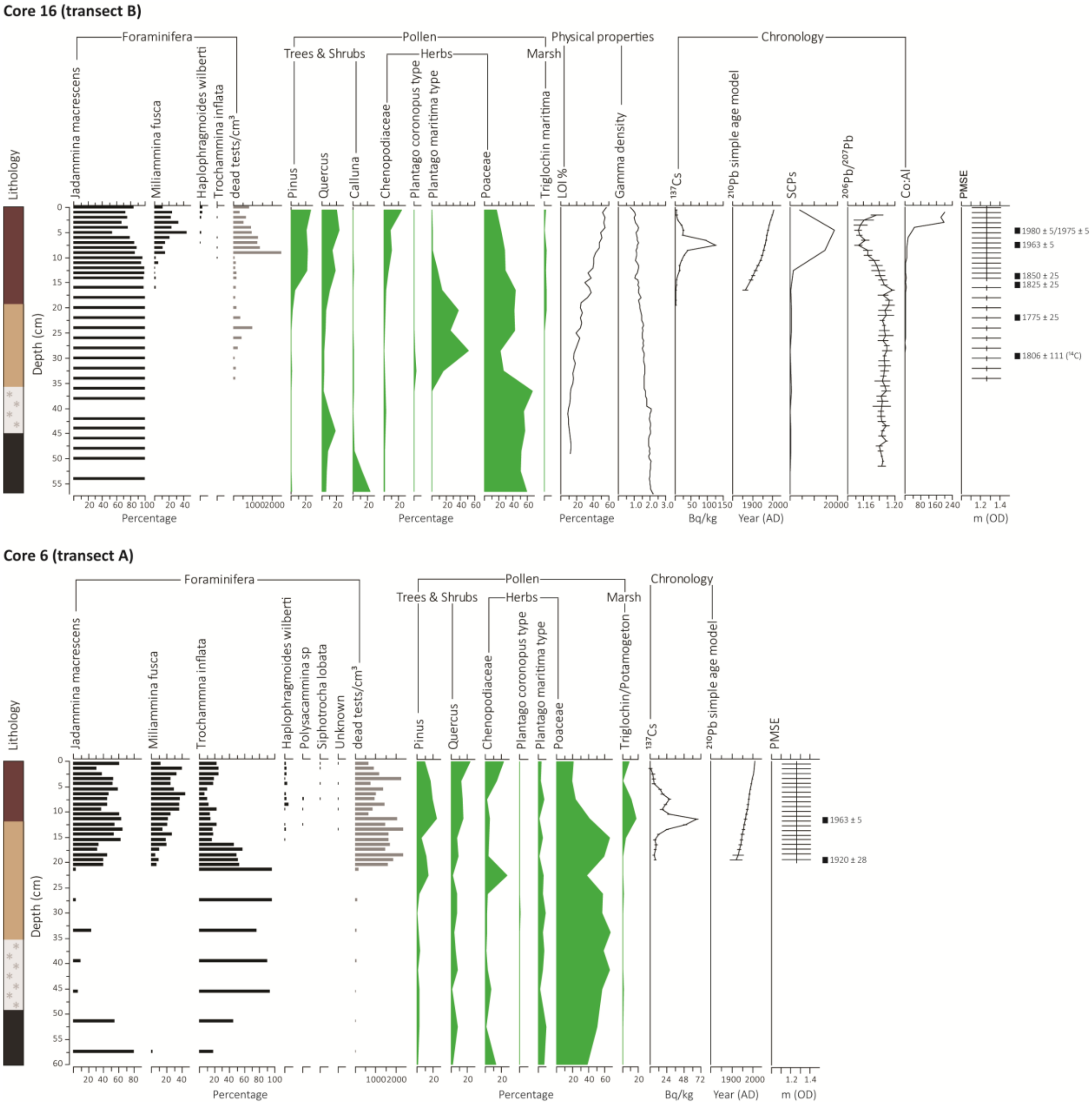
Core 16 (transect B)
Foraminifera
Pollen
Trees & Shrubs
Herbs
Marsh
Physical properties
Chronology
Lithology
Jadammina macrescens
Miliammina fusca
Haplophragmoides wilberti
Trochammina inflata
dead tests/cm³
Pinus
Quercus
Calluna
Chenopodiaceae
Plantago coronopus type
Plantago maritima type
Poaceae
Triglochin maritima
LOI %
Gamma density
137Cs
210Pb simple age model
SCPs
206Pb/207Pb
Co:Al
PMSE
Depth (cm)
Percentage
Bq/kg
Year (AD)
m (OD)
1980 ± 5/1975 ± 5
1963 ± 5
1850 ± 25
1825 ± 25
1775 ± 25
1806 ± 111 (14C)
Core 6 (transect A)
Foraminifera
Pollen
Trees & Shrubs
Herbs
Marsh
Chronology
Lithology
Jadammina macrescens
Miliammina fusca
Trochammina inflata
Haplophragmoides wilberti
Polysacammina sp
Siphotrocha lobata
Unknown
dead tests/cm³
Pinus
Quercus
Chenopodiaceae
Plantago coronopus type
Plantago maritima type
Poaceae
Triglochin/Potamogeton
137Cs
210Pb simple age model
PMSE
Depth (cm)
Percentage
Bq/kg
Year (AD)
m (OD)
1963 ± 5
1920 ± 28

Figure 5

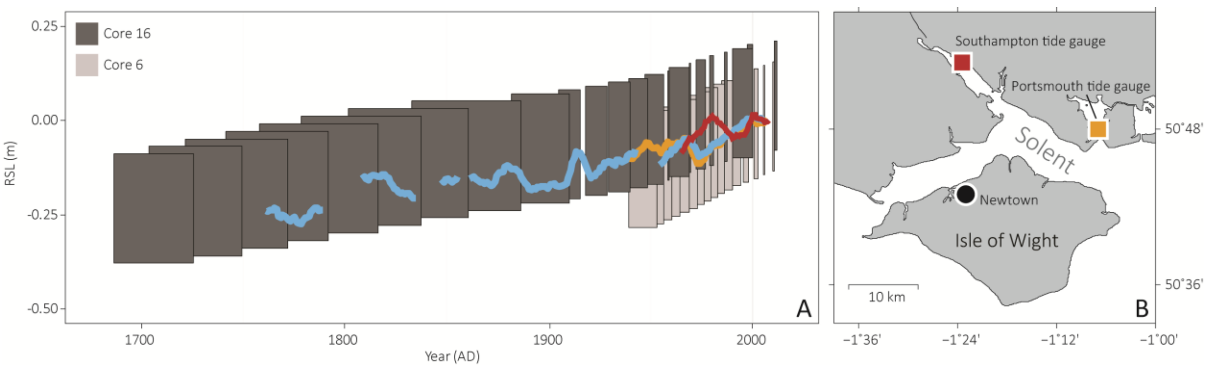

Core 16
Core 6
0.25
0.00
-0.25
-0.50
RSL (m)
1700
1800
1900
2000
Year (AD)
A
Southampton tide gauge
Portsmouth tide gauge
Solent
Newtown
Isle of Wight
10 km
50°48'
50°36'
−1°36'
−1°24'
−1°12'
−1°00'
B

Figure 6

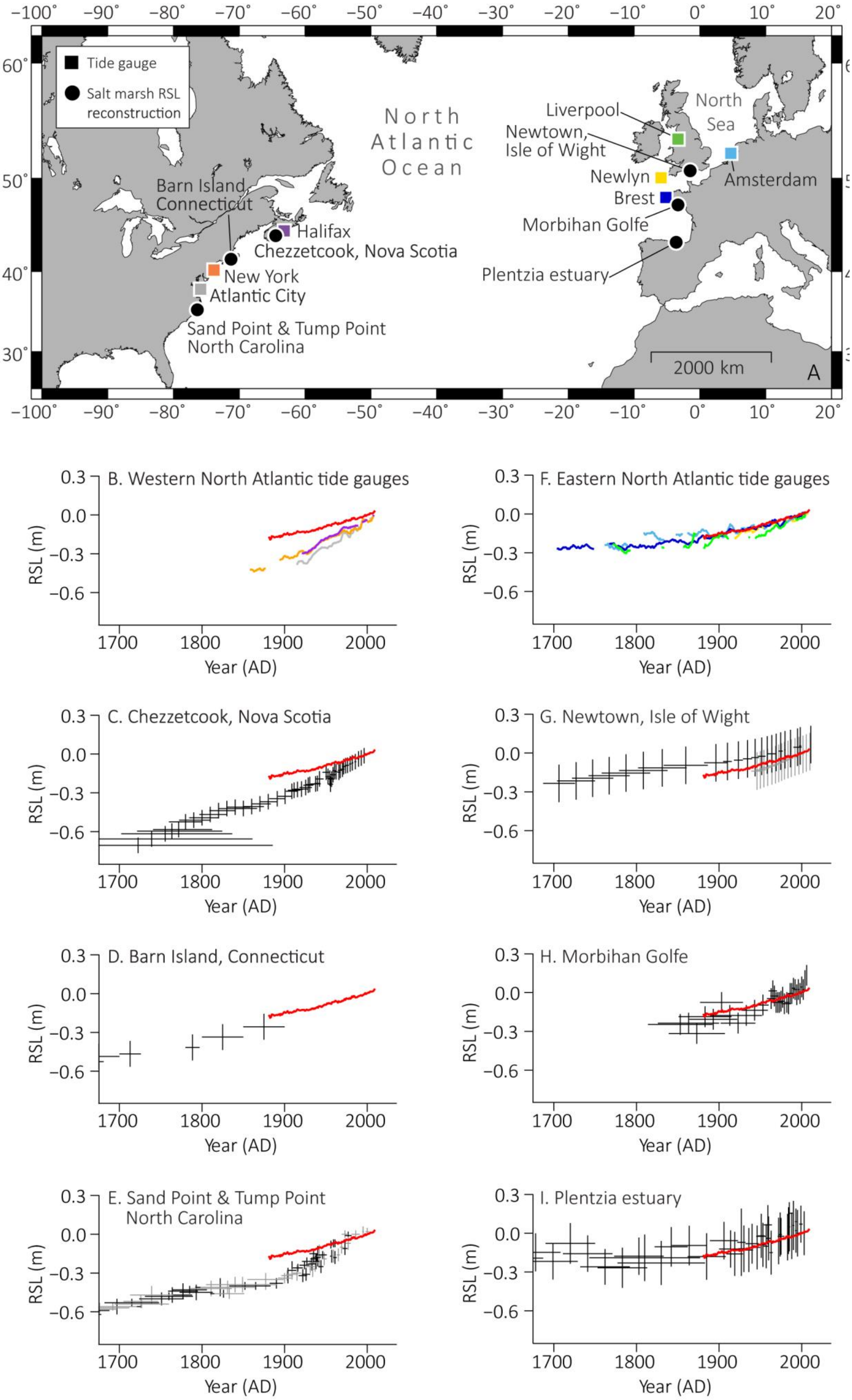
Tide gauge
Salt marsh RSL reconstruction
North Atlantic Ocean
North Sea
Liverpool
Newtown, Isle of Wight
Newlyn
Brest
Amsterdam
Morbihan Golfe
Plentzia estuary
Barn Island Connecticut
Halifax
Chezzetcook, Nova Scotia
New York
Atlantic City
Sand Point & Tump Point North Carolina
2000 km
A
B. Western North Atlantic tide gauges
C. Chezzetcook, Nova Scotia
D. Barn Island, Connecticut
E. Sand Point & Tump Point North Carolina
F. Eastern North Atlantic tide gauges
G. Newtown, Isle of Wight
H. Morbihan Golfe
I. Plentzia estuary
RSL (m)
Year (AD)

Figure 7

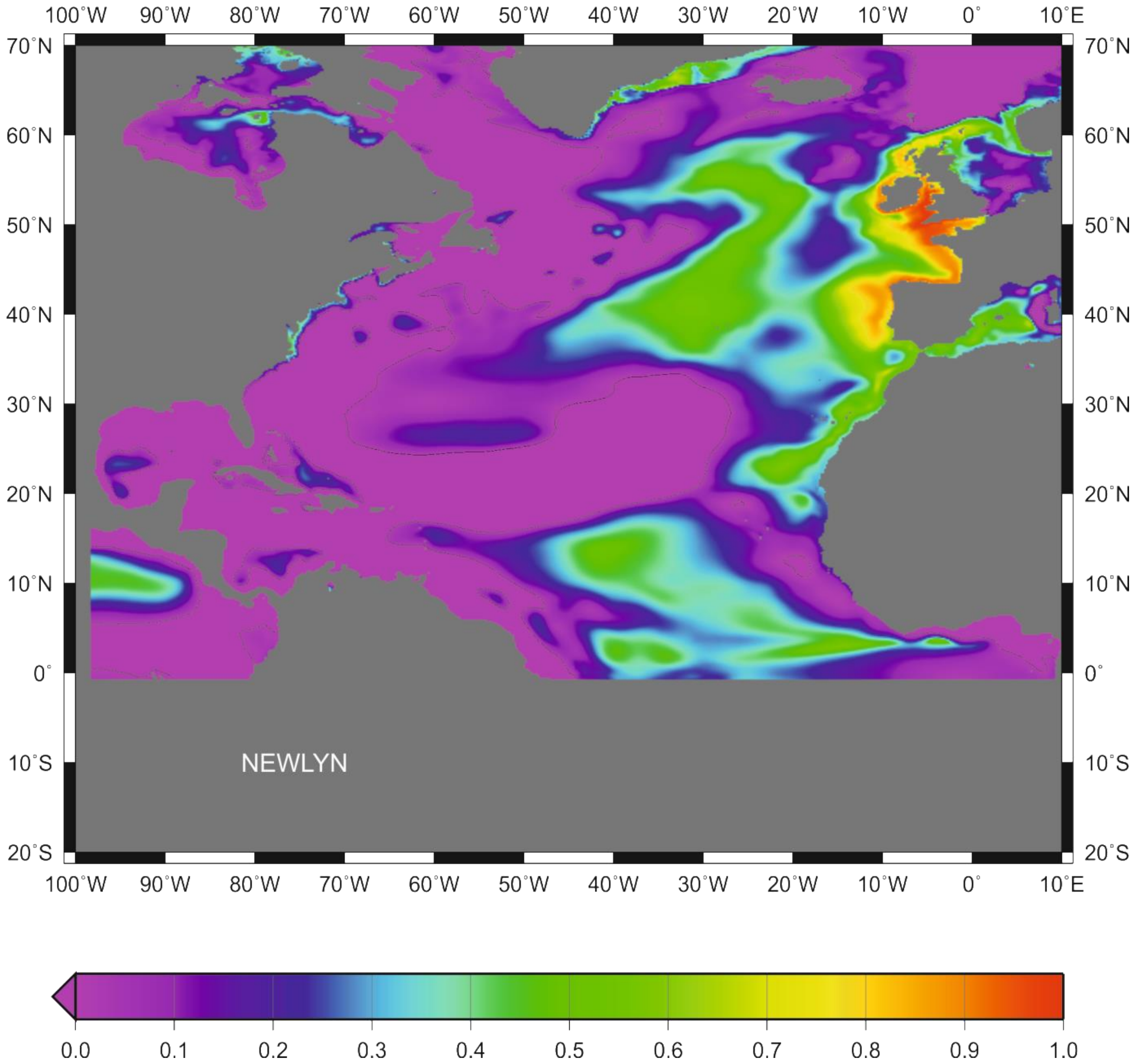
100°W 90°W 80°W 70°W 60°W 50°W 40°W 30°W 20°W 10°W 0° 10°E
70°N 60°N 50°N 40°N 30°N 20°N 10°N 0° 10°S 20°S
NEWLYN
0.0 0.1 0.2 0.3 0.4 0.5 0.6 0.7 0.8 0.9 1.0

Figure 8

SUPPLEMENTARY INFORMATION

Contrasting records of sea-level change in the eastern and western North Atlantic during the last 300 years

Long, A.J., Barlow, N.L.M., Gehrels, W.R., Saher, M.H., Woodworth, P.L, Scaife, R.G., Brain, M.J., Cahill, N.

Contents

Table S5	Modern foraminifera counts from Newtown marsh, with elevation in meters Ordnance Datum (OD)
Table S6	Fossil foraminifera counts for core NM-16
Table S7	Fossil foraminifera counts for core NM-6
Table S8	Pollen counts (in percentage) for core NM-16
Table S9	Pollen counts (in percentage) for core NM-6

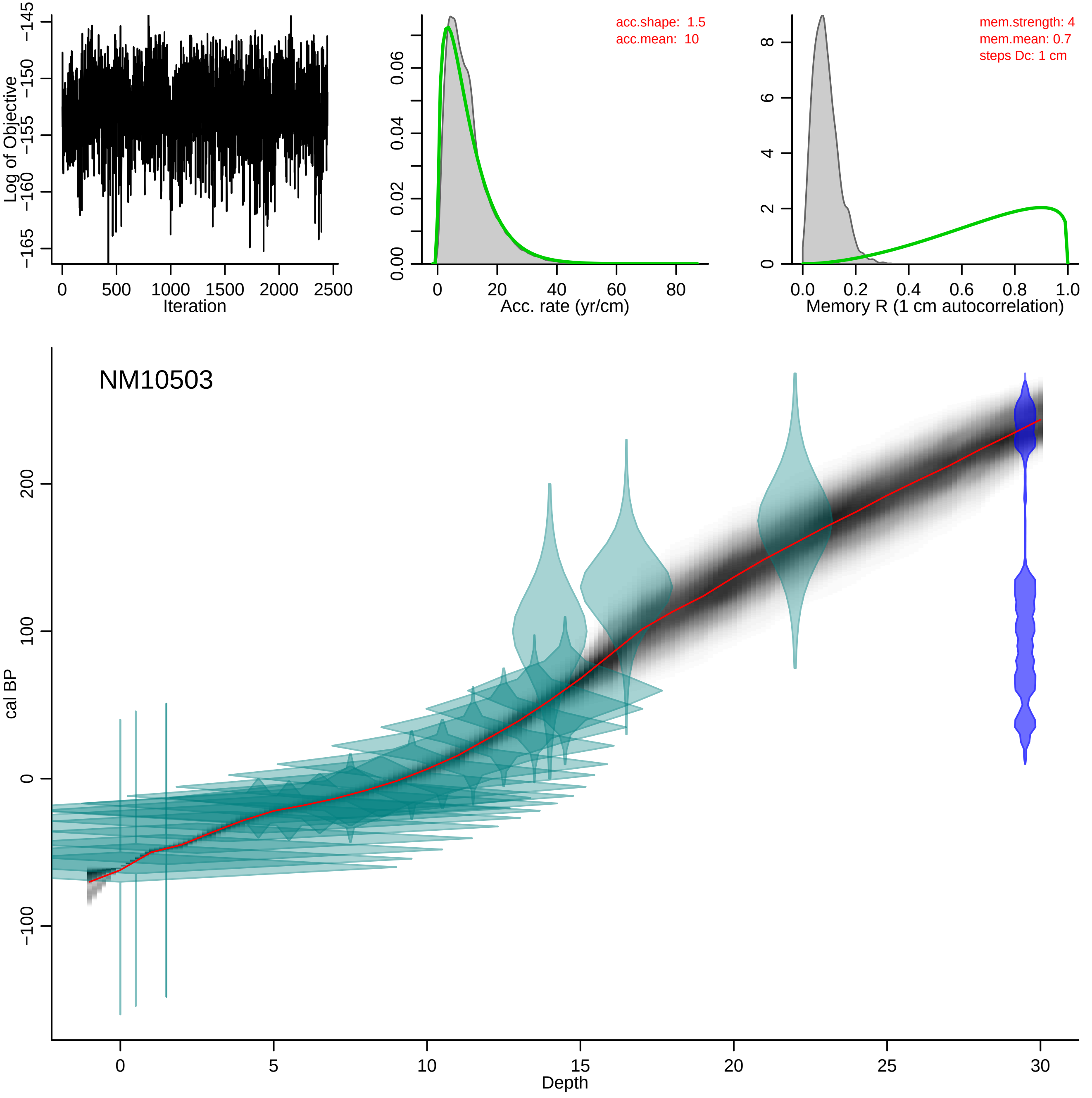

Log of Objective
Iteration
acc.shape: 1.5
acc.mean: 10
Acc. rate (yr/cm)
mem.strength: 4
mem.mean: 0.7
steps Dc: 1 cm
Memory R (1 cm autocorrelation)
NM10503
cal BP
Depth

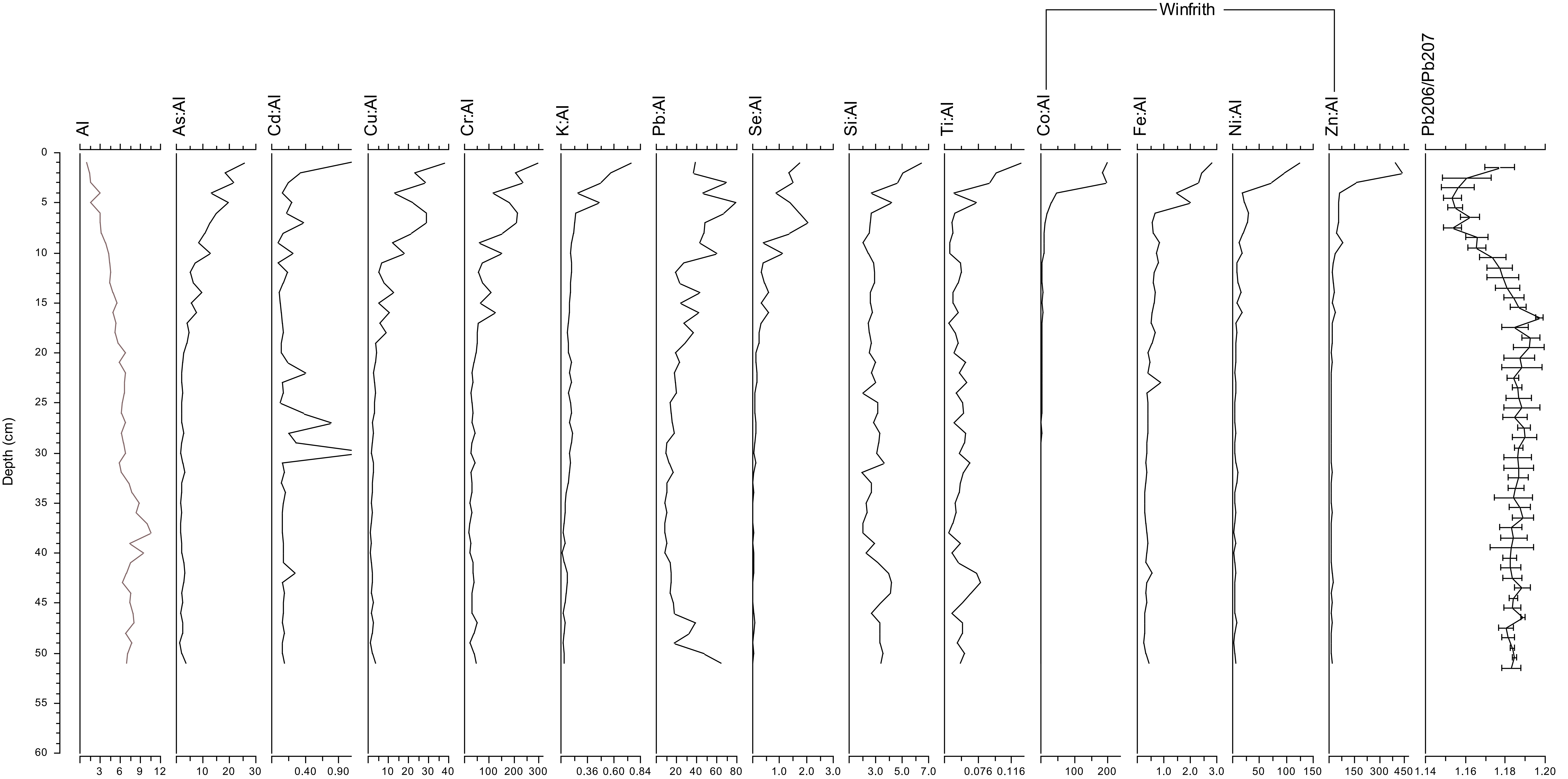

Winfrith
Al
As:Al
Cd:Al
Cu:Al
Cr:Al
K:Al
Pb:Al
Se:Al
Si:Al
Ti:Al
Co:Al
Fe:Al
Ni:Al
Zn:Al
Pb206/Pb207
Depth (cm)

Newtown East

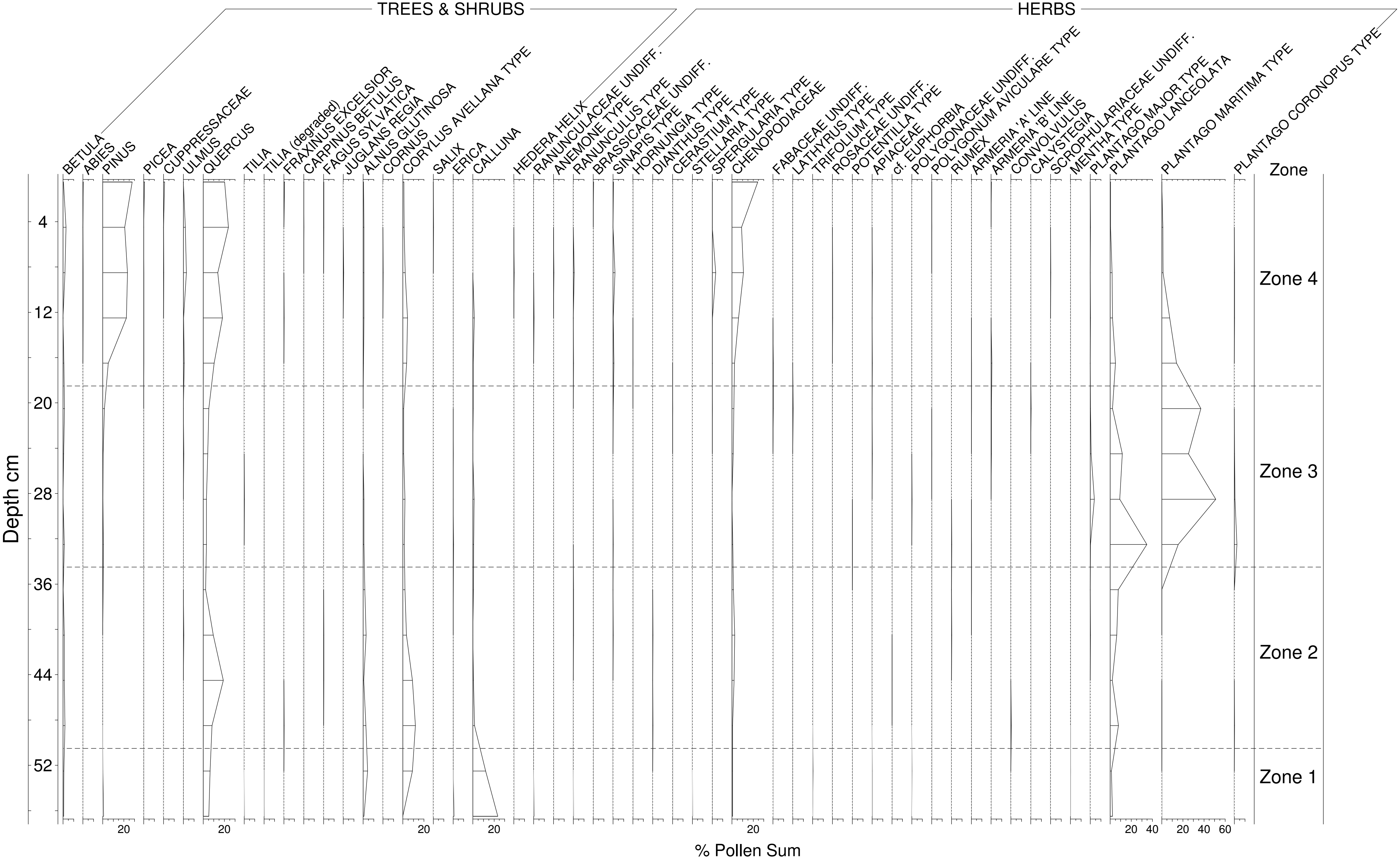

Newtown East Cont.

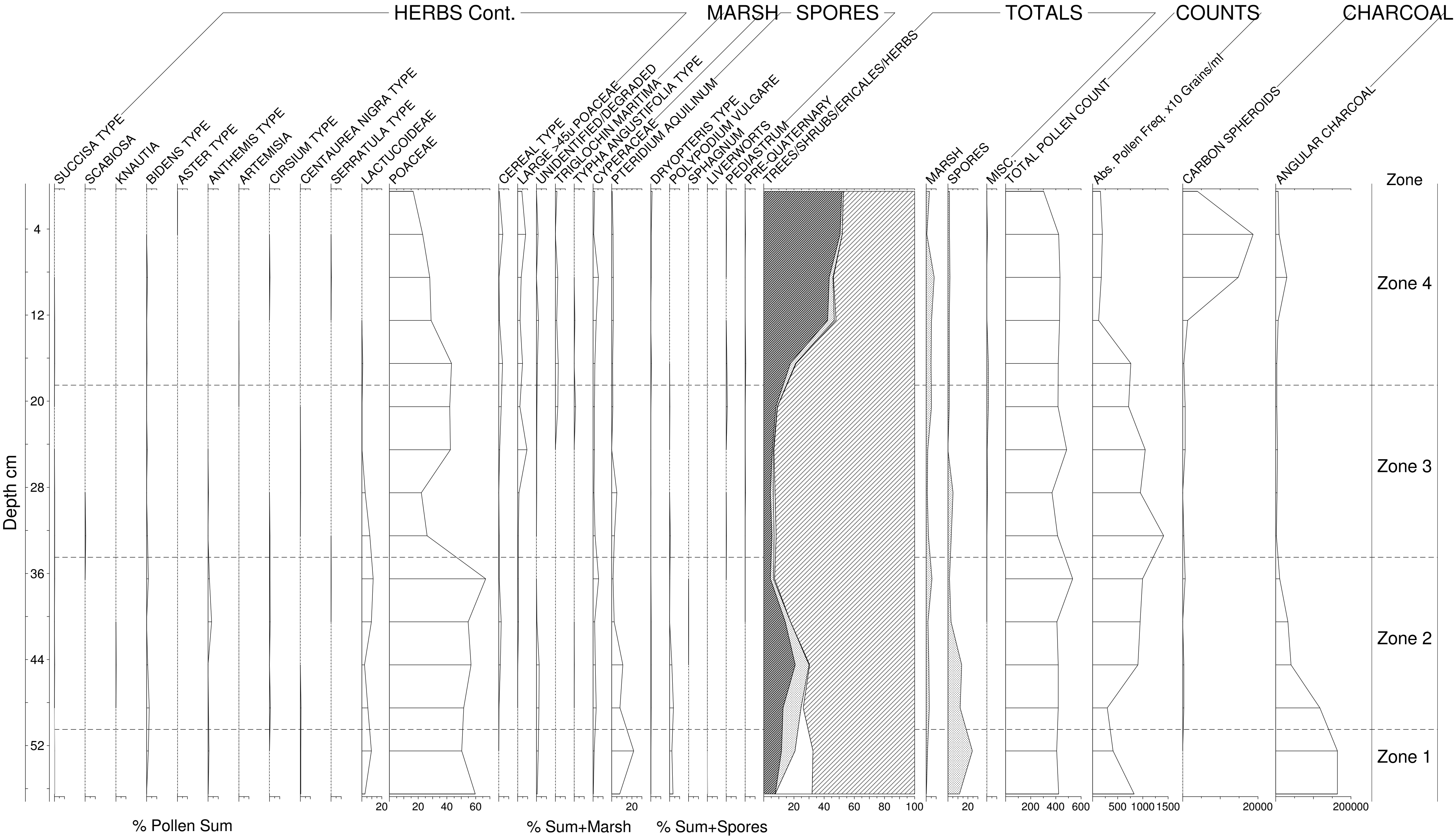

Rob Scaife 2010

Newtown East

Section 1

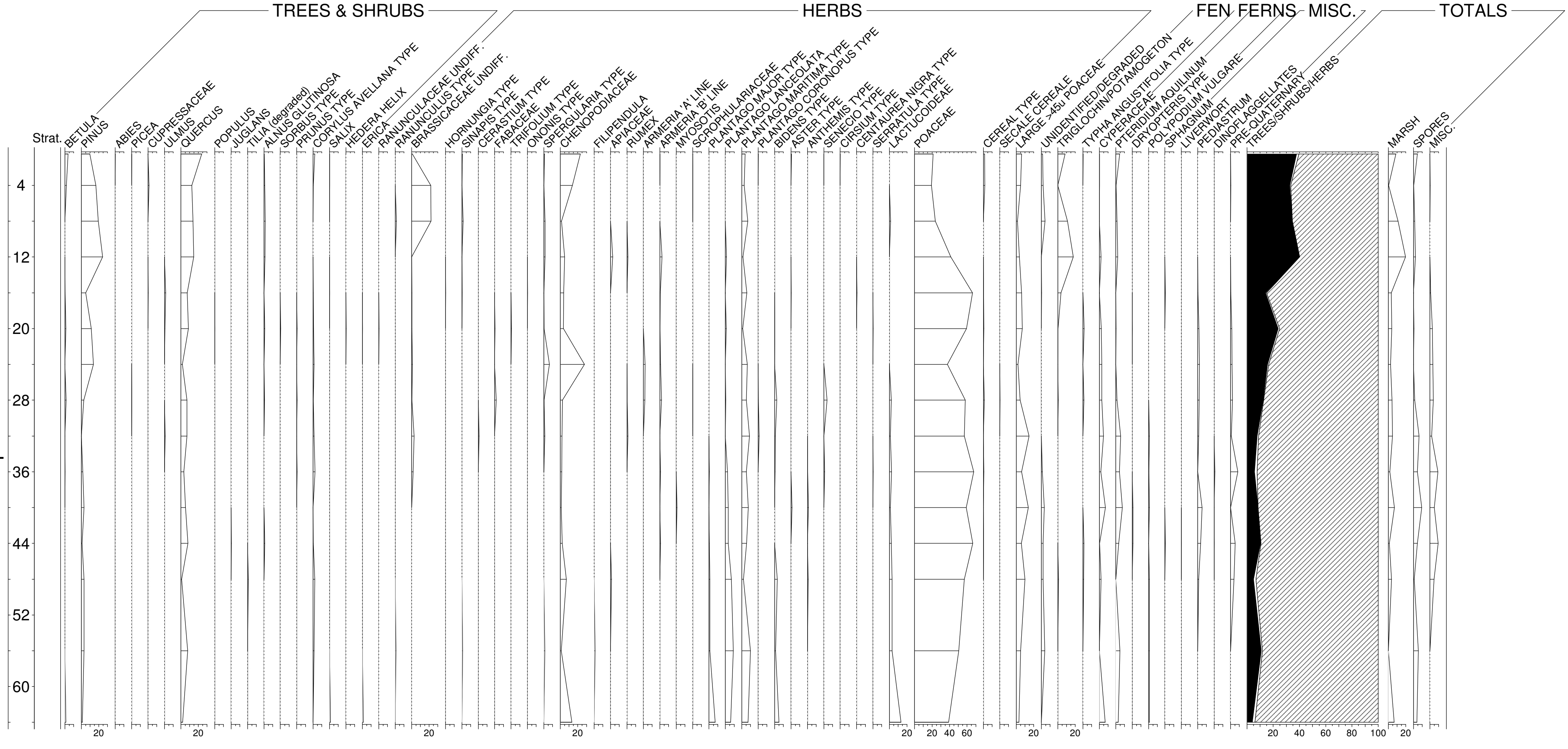

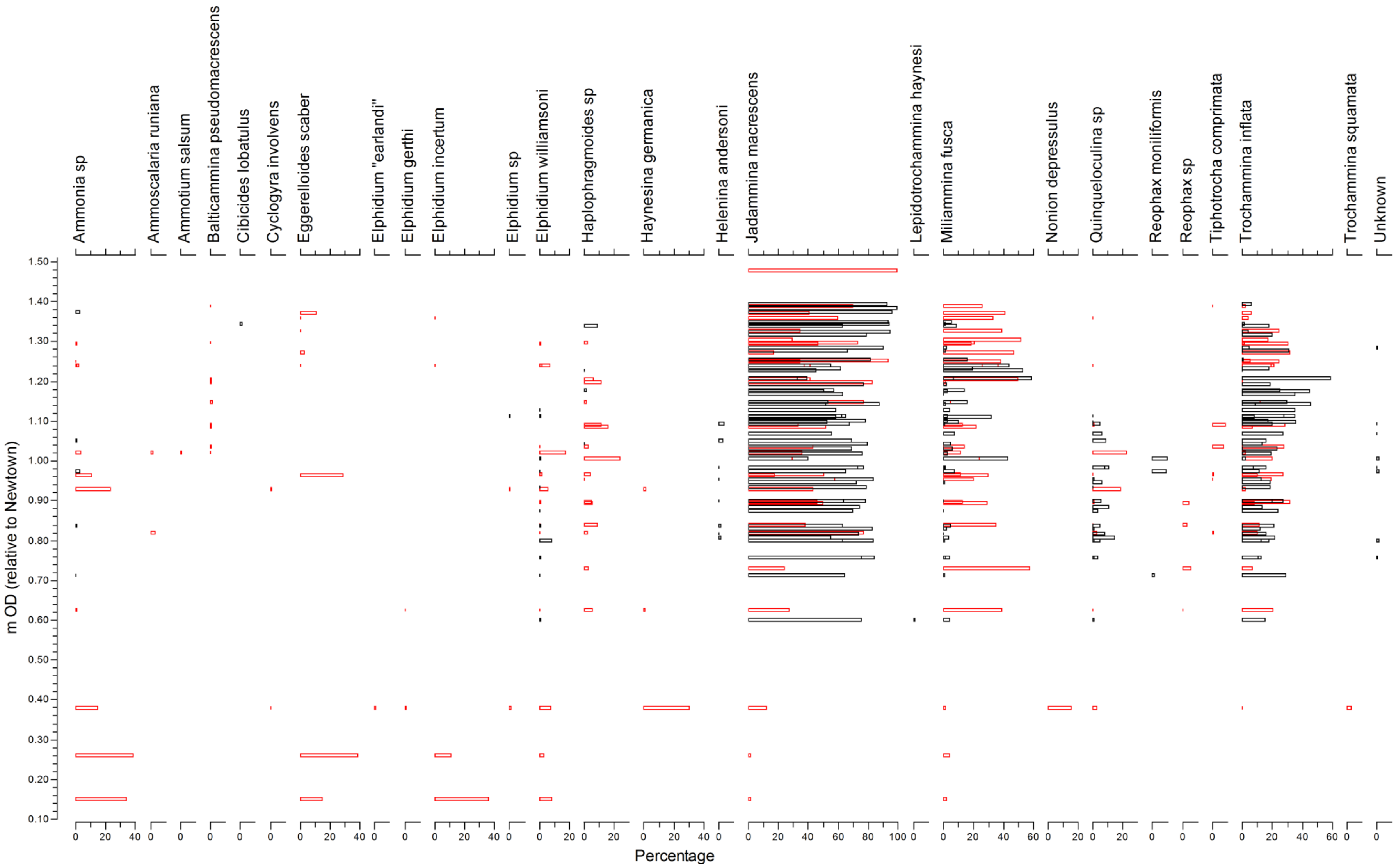

Ammonia sp
Ammoscalaria runiana
Ammotium salsum
Balticammina pseudomacrescens
Cibicides lobatulus
Cyclogyra involvens
Eggerelloides scaber
Elphidium "earlandi"
Elphidium gerthi
Elphidium incertum
Elphidium sp
Elphidium williamsoni
Haplophragmoides sp
Haynesina germanica
Helenina andersoni
Jadammina macrescens
Lepidotrochammina haynesi
Miliammina fusca
Nonion depressulus
Quinqueloculina sp
Reophax moniliformis
Reophax sp
Tiphotrocha comprimata
Trochammina inflata
Trochammina squamata
Unknown
m OD (relative to Newtown)
Percentage

Figure S5

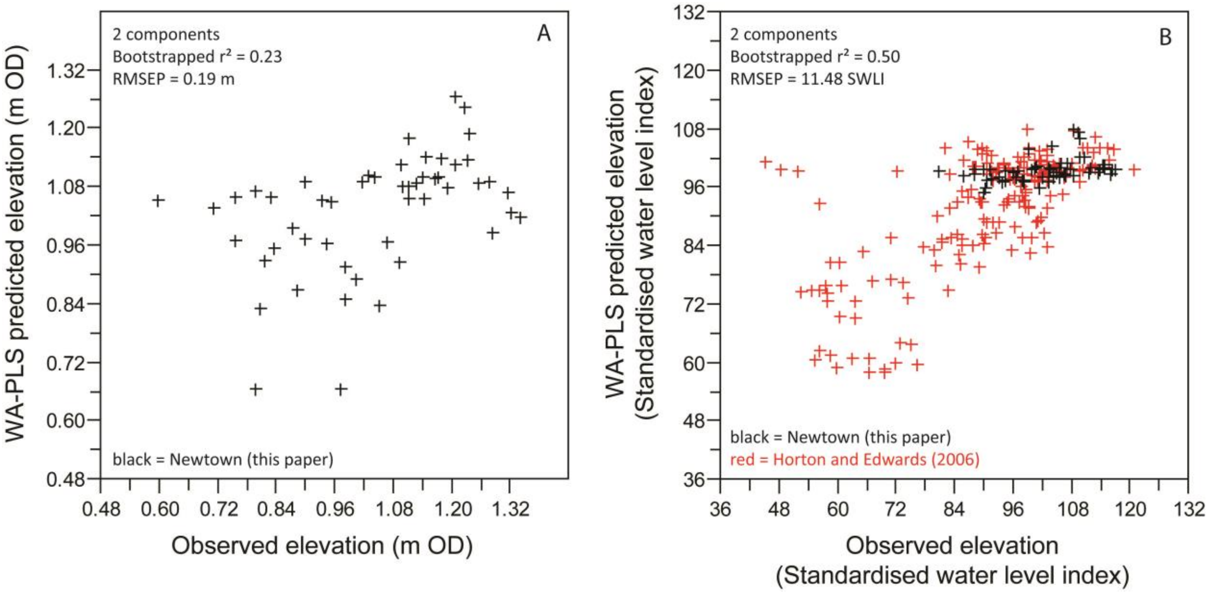
2 components
Bootstrapped r² = 0.23
RMSEP = 0.19 m
A
black = Newtown (this paper)
WA-PLS predicted elevation (m OD)
Observed elevation (m OD)
0.48
0.60
0.72
0.84
0.96
1.08
1.20
1.32
2 components
Bootstrapped r² = 0.50
RMSEP = 11.48 SWLI
B
black = Newtown (this paper)
red = Horton and Edwards (2006)
WA-PLS predicted elevation (Standardised water level index)
Observed elevation (Standardised water level index)
36
48
60
72
84
96
108
120
132

Figure S6

Alloc Number	Material ID code	Depth (cm)	AMS Lab number	% MC	% MC Error	online d^{13}C*	online d^{13}C error*	^{14}C Age	^{14}C Age error
1490.081	NM05.5	5.5	SUERC-31974	110.18	0.23	-28.4	0.5		
1490.081	NM09.5	9.5	SUERC-32115	169.36	0.94	-27.9	0.6		
1490.081	NM15.5	15.5	SUERC-31975	126.42	0.28	-28.0	0.5		
1490.081	NM21.5	21.5	SUERC-31976	106.89	0.22	-27.5	0.5		
1490.081	NM25.5	25.5	SUERC-31977	102.97	0.21	-26.9	0.5		
1490.081	NM25.5	25.5	SUERC-31978	103.41	0.21	-26.9	0.5		
1490.081	NM29.5	29.5	SUERC-31979	98.7	0.21	-26.2	0.5	105	17
1490.081	NM29.5	29.5	SUERC-31991	98.69	0.19	-26.2	0.5	106	16
1490.081	NM33.5	33.5	SUERC-31992	103.54	0.19	-27.3	0.5		
1490.081	NM36.5	36.5	SUERC-31993	101.49	0.21	-27.3	0.5		
1490.081	NM46.5	46.5	SUERC-31994	113.47	0.23	-27.3	0.5		

Material dated: unidentified plant macrofossil

Samples SUERC-31974 to SUERC-32012 underwent high precision AMS analysis at low current. $^{13}C/^{12}C$ ratios for these samples were measured on the SUERC AMS during 14C determination and were used to model $\delta^{13}C$ values by comparison to the Craig (1957) $^{13}C/^{12}C$ value for PDB. These values are shown outside the brackets and were considered the most appropriate to normalise ^{14}C data to $\delta^{13}C$VPDB‰ = -25, but are not necessarily representative of the $\delta^{13}C$ in the original sample material. The $\delta^{13}C$ values inside brackets (values given in table above) were measured on a dual inlet stable isotope mass spectrometer (VG OPTIMA) and are representative of $\delta^{13}C$ in the original, pre-treated sample material. The expertise and effort of M Currie (NRCF Environment) and P Ascough (SUERC) in preparing and analysing these samples are acknowledged. Online $\delta^{13}C$ by AMS was not undertaken on the remaining samples (SUERC-32502 and SUERC-32503).

Table S1

Compaction modelling and estimating Post-Depositional Lowering

Summary

No site-specific geotechnical data were available for our study site in the Newtown Estuary and no samples were collected for laboratory geotechnical testing. Post-Depositional Lowering (PDL) in Core NM-16 was instead estimated using a UK database of the compression properties of low energy intertidal sediments and the compression and decompaction models developed by Brain *et al*. (2011; 2012).

The model uses the same approach and algorithms as Brain *et al*. (2012), with exceptions detailed below. However, in contrast, the model is run here using loss on ignition (LOI) values measured in core NM-16 (Figure 5) to estimate downcore bulk density and compression properties. We use a layer thickness of 0.01 m and assume a groundwater table at the ground surface, as seems reasonable from the hydrological conditions observed at our study site.

To explore and estimate uncertainty in model outputs resulting from regression model error and the inherent uncertainty of some of our assumptions regarding compression properties, we use a repeat-iteration, stochastic (Monte-Carlo) approach to propagate uncertainty through the model into predicted PDL. We run the model 1000 times and calculate the mean and standard deviation of PDL in each layer. The PDL profile is displayed in Figure S6.

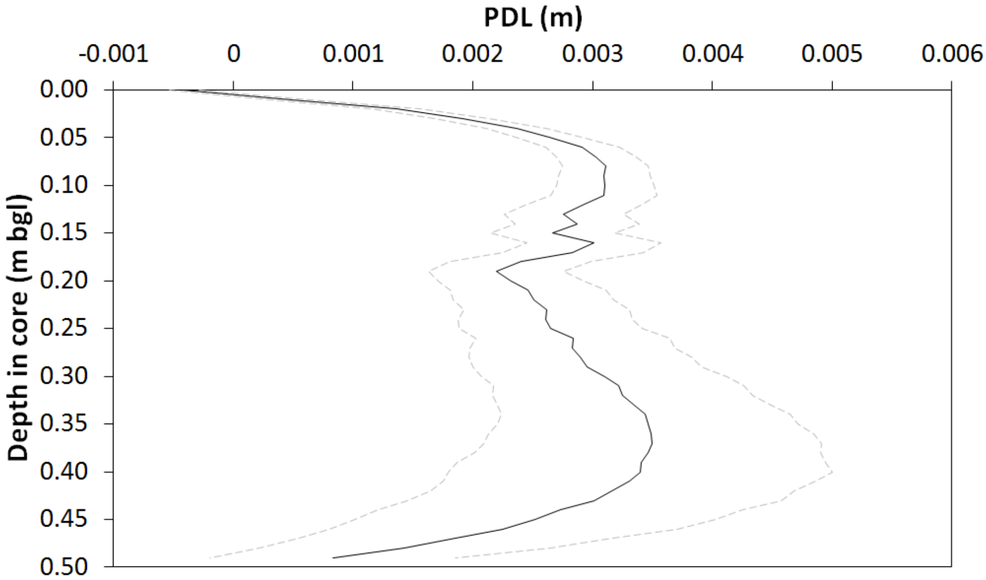

Figure S7. Predicted post-depositional lowering (PDL) with depth for core NM-16. Black line indicates the mean of 1000 model runs and dashed grey lines represent the standard deviation thereof.

UK compression database

The database comprises results of oedometer compression tests undertaken on sediment samples obtained from four UK low energy intertidal sites:

- Cowpen Marsh, Tees Estuary, NE England, *n* = 30, LOI, range = 7 – 40 % (Brain *et al*., 2011; 2012);
- Roudsea Marsh, Leven Estuary, Cumbria, England, *n* = 6, LOI range = 3 – 14 % (Brain *et al*., 2012);

- Thornham Marsh, North Norfolk, England, n = 6, LOI range = 1 – 30 % (Brain *et al.*, 2012); and
- Loch Laxford, NW Scotland, n = 17, LOI range = 40 – 86 % (Cullen, 2012).

Whilst these sites vary in geomorphic setting, hydrographic conditions and eco-sedimentological characteristics, statistically significant predictive relationships have been observed between key physical properties (notably LOI) and compression properties (Brain *et al.*, 2012; Cullen, 2012). Hence, whilst we have not obtained site-specific compression properties for input into compression/decompaction models from the Isle of Wight, we were able to estimate e_1 (voids ratio at 1 kPa), C_r (compressibility at effective stresses less than the yield stress) and C_c (compressibility at effective stresses greater than the yield stress) from their relationships with LOI, as observed at other UK sites. In addition, to permit estimation of downcore bulk density, G_s (specific gravity) was also predicted from LOI.

Regression model equations and error estimation

Where appropriate, we used the standard error of the estimate as our regression model error. However, following Brain *et al*. (2012), where the form of the residuals deviates from a normal distribution (i.e. if the residuals failed a Shapiro-Wilk normality test), we used a uniformly distributed error term (± half the range of the modelled residuals). Predictive relationships and regression model error estimations are provided in Tables S2 and S3 respectively.

Table S2. Predictive equations used to estimate key compression and physical properties using measured downcore loss on ignition values.

Equation	r^2_{adj}	p
$G_s = 2.7458 + (-0.0144 \cdot \mathrm{LOI})$	0.96	<0.0001
$e_1 = \dfrac{9.731}{1 + \exp\left(-\dfrac{\mathrm{LOI} - 25.3832}{8.6875}\right)}$	0.94	<0.0001
$C_r = \dfrac{0.8944}{1 + \exp\left(-\dfrac{\mathrm{LOI} - 35.0381}{4.3231}\right)}$	0.90	<0.0001
$C_c = (0.0777 \cdot \mathrm{LOI}) - 0.1859$	0.92	<0.0001

Table S3. Summary of error terms for regression models used in compression and decompaction modelling.

Predicted (predictor) variable	Residuals passed Shapiro-Wilk normality test?	Regression model error distribution	± error term
Specific gravity (loss on ignition)	Yes	Normal	0.0689
e_1 (loss on ignition)	Yes	Normal	0.7584
C_r (loss on ignition)	No	Uniform	0.40
C_c (loss on ignition)	No	Uniform	1.38

Brain *et al*. (2012) noted that compressive yield stress is controlled by local factors that do not necessarily transcend site boundaries, such as tidal setting (flooding frequency and duration) and eco-sedimentary conditions (the presence or absence of surface biomass), both of which control the potential for desiccation and overconsolidation at the depositional surface. Hence, 'universal' empirical relationships with LOI do not exist, though relationships can be observed on a site-by-site basis. In the absence of site-specific data, we were unable to define predictive relationships between compressive yield stress and elevation within the intertidal zone (cf. Brain *et al*., 2012). We therefore estimate yield stress based on the lithologies and flooding characteristics of similar contemporary surface materials in the compression database for which we have observed sediment yield stresses.

For the more organic salt marsh sediments observed in the upper 0.3 m of the core, we assign a uniform distribution of yield stress values to the sediments based on the minimum (3kPa, Cowpen Marsh) and maximum (10 kPa, Loch Laxford) values observed in our database for high marsh lithologies displaying similar values (LOI > 20 %). To consider the potential presence of fully normally consolidated sediments in the organic high marsh, we extended the lower bound of this distribution to 0.5 kPa. For the organic silts encountered at depths > 0.3 m below ground level that typically display greater yield stresses in our database, we defined a uniform distribution of 6 to 14 kPa. Due to the extremely low effective stresses experienced within the core, estimations of PDL demonstrate no sensitivity to yield stress, since no yield stress less than this effective stress value are observed in our database.

References

Cullen, B.J. 2012. Decompacting a Late Holocene sea-level record from Loch Laxford, northwest Scotland. Unpublished MRes Thesis, Durham University, UK.

Brain, M.J., Long, A.J., Petley, D.N., Horton, B.P., Allison, R.J., 2011. Compression behaviour of minerogenic low energy intertidal sediments. Sedimentary Geology, 233, 28 –41.

Brain, M.J., Long, A.J, Woodroffe, S.A., Petley, D.N., Milledge, D.G., Parnell, A.C., 2012. Modelling the effects of sediment compaction on salt marsh reconstructions of recent sea-level rise. Earth and Planetary Science Letters, 345-348, 180-193.

RSL (m)	RSL Error (m)	Age (yr AD)	Plus age error (yr)	Minus age error (yr)	Core
0.065	0.145	2011	0.5	0.5	NM-16
0.055	0.145	1998.3	1.3	1.3	NM-16
0.045	0.145	1994.9	5.1	4.9	NM-16
0.035	0.145	1986.5	4.5	0.5	NM-16
0.025	0.145	1979.7	0.7	0.7	NM-16
0.015	0.145	1974.5	2.5	2.5	NM-16
0.005	0.145	1969.1	4.9	0.1	NM-16
-0.005	0.145	1963.8	0.2	4.8	NM-16
-0.015	0.145	1958.3	4.7	0.3	NM-16
-0.025	0.145	1951.6	0.4	4.6	NM-16
-0.035	0.145	1943.6	5.4	4.6	NM-16
-0.045	0.145	1934.4	9.6	5.4	NM-16
-0.055	0.145	1923.4	9.6	5.4	NM-16
-0.065	0.145	1910.2	9.8	5.2	NM-16
-0.075	0.145	1896.2	10.8	14.2	NM-16
-0.095	0.145	1859.7	18.3	26.7	NM-16
-0.115	0.145	1831.3	25.7	29.3	NM-16
-0.135	0.145	1808.3	30.7	29.3	NM-16
-0.155	0.145	1787.3	25.7	29.3	NM-16
-0.175	0.145	1766.9	30.1	24.9	NM-16
-0.195	0.145	1747	30	25	NM-16
-0.215	0.145	1726.9	27.1	22.9	NM-16
-0.235	0.145	1706.3	15.7	19.3	NM-16
0.01	0.145	2009	0.5	0.5	NM-6
0	0.145	2005.57	0.38	0.38	NM-6
-0.01	0.145	2001.5	0.83	0.83	NM-6
-0.02	0.145	1996.73	1.35	1.35	NM-6
-0.03	0.145	1991.92	1.88	1.88	NM-6
-0.04	0.145	1987.33	2.39	2.39	NM-6
-0.05	0.145	1983.38	2.83	2.83	NM-6
-0.06	0.145	1979.17	3.29	3.29	NM-6
-0.07	0.145	1975.62	3.68	3.68	NM-6
-0.08	0.145	1972.14	4.07	4.07	NM-6
-0.09	0.145	1968.21	4.5	4.5	NM-6
-0.1	0.145	1963.99	4.97	4.97	NM-6
-0.11	0.145	1958.72	5.55	5.55	NM-6
-0.12	0.145	1954.31	6.04	6.04	NM-6
-0.13	0.145	1949.98	6.51	6.51	NM-6
-0.14	0.145	1945.98	6.95	6.95	NM-6
-0.15	0.145	1940.93	7.51	7.51	NM-6
-0.16	0.145	1935.38	8.12	8.12	NM-6
-0.17	0.145	1929.92	25.35	25.35	NM-6
-0.18	0.145	1920.48	28.38	28.38	NM-6

Table S4

#	Code	Elevation (m OD)	Jadammina macrescens	Trochammina inflata	Miliammina fusca	Quinqueloculina sp	Haplophragmoides wilberti	Lepidotrochammina haynesi	Reophax cf catella	Helenina andersoni	Ammonia sp.	Cibicides lobatulus	Elphidium williamsoni	Elphidium sp	Cornuspira sp.	Haynesina germanica	Unknown	Total counts
1	NM09-s69	1.395	14	1														15
2	NM09-s68	1.383	4															4
3	NM09-s37	1.371	28								1							29
4	NM09-s67	1.348	31		2													33
5	NM09-s36	1.343	55	1	1							1						58
6	NM09-s38	1.339	14	4	2		2											22
7	NM09-s66	1.323	108	5														113
8	NM09-s35	1.317	55	14														69
9	NM09-s65	1.283	67	4	2												1	74
10	NM09-s34	1.278	74	35	2													111
11	NM09-s64	1.256	245	4	49													298
12	NM09-s62	1.237	361	1	290													652
13	NM09-s33	1.232	388	114	123													625
14	NM09-s63	1.226	270	3	315		4										1	593
15	NM09-s32	1.208	75	134	17													226
16	NM09-s61	1.207	83	2	123													208
17	NM09-s26	1.192	244	61	9													314
18	NM09-s59	1.178	55	25	14		2											96
19	NM09-s25	1.173	57	51	4													112
20	NM09-s30	1.168	69	39	1													109
21	NM09-s56	1.147	72	41	22													135
22	NM09-s24	1.143	324	35	7								1				1	368
23	NM09-s57	1.142	62	55	2													119
24	NM09-s55	1.127	120	73	10								1					204
25	NM09-s27	1.112	56	24	3								1	1				85
26	NM09-s23	1.112	71	40	1	1												113
27	NM09-s60	1.111	42	6	23													71
28	NM09-s29	1.100	94	21	4													119
29	NM09-s53	1.096	155	106	31	2												294
30	NM09-s22	1.092	377	114	6	28				23					2		2	552
31	NM09-s52	1.069	57	28	8	7											1	101
32	NM09-s21	1.051	60	14		8				3	1							86
33	NM09-s51	1.042	117	20	8		1											146
34	NM09-s14	1.030	61	21	6													88
35	NM09-s50	1.018	74	19	3													96
36	NM09-s28	1.005	61	4	66				15				2				3	151
37	NM09-s20	0.983	113	25	2	13											1	154
38	NM09-s49	0.982	80	8	2	12				1								103
39	NM09-s58	0.974	85	15	10				12		4		1				3	130

Table S5 - Newtown modern foraminifera

40	NM09-s13	0.953	419	67	1	6				4							1	498
41	NM09-s48	0.945	45	12	1	4												62
42	NM09-s47	0.933	114	27		1							1					143
43	NM09-s12	0.900	134	58	2	13				1					1			209
44	NM09-s46	0.899	118	31	1													150
45	NM09-s19	0.883	60	11		9												80
46	NM09-s45	0.873	104	36	1	6							1					148
47	NM09-s41	0.836	59	20	5	5				2	1		1					93
48	NM09-s44	0.829	67	10	2	1												80
49	NM09-s11	0.816	137	30	1	16				1								185
50	NM09-s42	0.807	99	40	7	27				3					1			177
51	NM09-s10	0.799	157	25	3	2												187
52	NM09-s40	0.797	58	17	1	5							8				2	91
53	NM09-s39	0.756	82	11	2	1											1	97
54	NM09-s18	0.756	71	12	4	4							1				1	93
55	NM09-s31	0.712	227	104	4				6	1	2		3			1	1	349
56	NM09-s43	0.599	63	13	4	1		1					1					83

Table S5 - Newtown modern foraminifera

Depth (cm)	Jadammina macrescens	Trochammina inflata	Miliammina fusca	Haplophragmoides wilberti	Lepidothrochammina haynesi	
0	180	2	26	13	1	
1	126		43	8		
2	246	2	73	5		
3	80		41	1		
4	177		56			
5	64		53	2		
6	125	1	33			
7	134		23	1		
8	153	1	19			
9	199		35			
10	90	1	2			
11	124		7			
12	107		1			
13	178		1			
14	156		3			
16	141		2			
18	96					
20	228					
22	366		1			
24	501					
26	91					
28	120					
30	55					
32	133					
34	95					
36	8					
38	8					
40						No tests
42	5					
44	2					
46	5					
48	1					
50	1					
52						No tests
54	1					
56						No tests

Table S6 - NM-16 fossil foraminifera

Depth (cm)	Jadammina macrescens	Trochammna inflata	Miliammina fusca	Haplophragmoides wilberti	Siphotrocha lobata	Polysacammina sp	Unknown
0	90	34	18	2	1		2
1	71	58	92	6	1	1	
2	55	38	49	4			
3	151	55	73	3		1	
4	87	31	42	5	1		2
5	51	9	26				
6	60	9	58	2			
7	54	13	45	3	1	2	1
8	161	46	133	18	1		1
9	39	24	39	1		1	1
10	49	11	20				
11	164	38	56	1			
12	101	43	39	1		1	
13	96	26	22	3			1
14	55	19	28				
15	64	17	20	1			
17	236	426	76	2	1		
19	93	120	22				
21	11	298					
27	6	177					
33	23	73					
39	12	109					
45	3	48					

Table S7 - NM-6 fossil foraminifera

Depth	BETULA	ABIES	PINUS	PICEA	CUPPRESSACEAE	ULMUS	QUERCUS	TILIA	TILIA (degraded)	FRAXINUS EXCELSIOR	CARPINUS BETULUS	FAGUS SYLVATICA	JUGLANS REGIA	ALNUS GLUTINOSA	CORNUS	CORYLUS AVELLANA TYPE	SALIX	ERICA	CALLUNA
0.5	0.34	0.34	27.74	0.68	1.03	0.00	20.21	0.00	0.00	0.68	0.00	0.34	0.00	0.34	0.00	1.03	0.00	0.00	0.00
4.5	2.86	0.00	20.76	0.00	0.00	1.91	23.87	0.00	0.00	0.00	0.24	0.24	0.00	0.72	0.00	1.19	0.24	0.00	0.00
8.5	1.75	0.25	23.31	0.25	0.25	2.76	13.80	0.00	0.00	0.00	0.00	0.00	0.30	0.75	0.25	2.20	0.00	0.00	0.00
12.5	0.00	0.25	22.36	0.25	0.00	0.25	18.18	0.00	0.00	0.25	0.00	0.00	0.00	0.74	0.00	4.42	0.00	0.00	1.23
16.5	0.75	0.00	5.28	0.25	0.00	0.75	10.30	0.00	0.00	0.00	0.00	0.00	0.00	0.25	0.00	3.52	0.00	0.00	0.25
20.5	1.27	0.00	1.52	0.00	0.00	0.00	5.32	0.00	0.00	0.00	0.00	0.00	0.00	0.00	0.00	0.76	0.00	0.00	0.25
24.5	0.63	0.00	0.42	0.00	0.00	0.42	4.18	0.00	0.00	0.00	0.00	0.00	0.00	0.00	0.00	0.84	0.00	0.21	0.00
28.5	0.00	0.00	0.27	0.00	0.00	0.00	3.01	0.27	0.00	0.00	0.00	0.00	0.00	0.82	0.00	1.91	0.00	0.00	1.09
32.5	1.23	0.00	0.49	0.00	0.00	0.00	2.96	0.00	0.00	0.00	0.00	0.00	0.00	0.74	0.00	1.48	0.00	0.49	0.74
36.5	0.20	0.00	0.40	0.00	0.00	0.00	2.19	0.00	0.00	0.00	0.00	0.00	0.00	1.59	0.00	1.99	0.00	0.20	0.60
40.5	1.25	0.00	0.00	0.00	0.00	0.50	9.48	0.00	0.00	0.00	0.00	0.25	0.00	2.74	0.00	3.49	0.00	0.00	0.00
44.5	1.23	0.00	0.00	0.00	0.00	0.00	18.92	0.00	0.00	0.00	0.00	0.25	0.00	0.49	0.00	9.09	0.00	0.00	0.49
48.5	1.72	0.00	0.00	0.00	0.00	0.00	8.37	0.00	0.00	0.25	0.00	0.00	0.00	2.46	0.00	11.82	0.00	0.00	1.48
52.5	0.75	0.00	0.25	0.00	0.00	0.00	6.47	0.00	0.00	0.00	0.00	0.00	0.00	4.23	0.00	8.96	0.00	0.00	11.94
56.5	0.47	0.00	0.71	0.00	0.00	0.00	5.21	0.24	0.24	0.00	0.00	0.00	0.00	0.71	0.00	0.00	0.00	0.95	23.46

Table S8 - NM-16 pollen (percentages)

Depth	HEDERA HELIX	RANUNCULACEAE UNDIFF.	ANEMONE TYPE	RANUNCULUS TYPE	BRASSICACEAE UNDIFF.	SINAPIS TYPE	HORNUNGIA TYPE	DIANTHUS TYPE	CERASTIUM TYPE	STELLARIA TYPE	SPERGULARIA TYPE	CHENOPODIACEAE	FABACEAE UNDIFF.	LATHYRUS TYPE	TRIFOLIUM TYPE	ROSACEAE UNDIFF.	POTENTILLA TYPE	APIACEAE	cf. EUPHORBIA
0.5	0.00	0.00	0.00	0.00	0.34	0.34	0.00	0.00	0.00	0.00	0.34	24.32	0.00	0.00	0.00	0.00	0.00	0.00	0.00
4.5	0.00	0.00	0.00	0.00	0.00	0.00	0.00	0.00	0.00	0.00	0.00	9.07	0.00	0.00	0.00	0.00	0.00	0.00	0.00
8.5	0.25	0.00	0.25	0.75	0.00	1.75	0.00	0.00	0.00	0.00	3.26	10.78	0.00	0.00	0.00	0.25	0.00	0.25	0.00
12.5	0.00	0.25	0.00	0.00	0.00	0.25	0.00	0.00	0.00	0.00	0.25	6.14	0.00	0.00	0.00	0.25	0.00	0.00	0.00
16.5	0.00	0.00	0.00	0.25	0.00	0.75	0.25	0.00	0.00	0.00	0.00	2.26	0.25	0.00	0.00	0.00	0.00	0.25	0.00
20.5	0.00	0.00	0.00	0.00	0.00	0.25	0.00	0.00	0.25	0.00	0.25	1.77	0.25	0.25	0.00	0.00	0.00	0.00	0.00
24.5	0.00	0.00	0.00	0.00	0.00	0.00	0.00	0.00	0.00	0.00	0.00	1.04	0.00	0.00	0.00	0.00	0.00	0.21	0.00
28.5	0.00	0.00	0.00	0.00	0.00	0.00	0.00	0.00	0.00	0.00	0.00	0.00	0.00	0.00	0.00	0.00	0.00	0.00	0.00
32.5	0.00	0.00	0.00	0.00	0.00	0.25	0.00	0.00	0.00	0.00	0.00	0.74	0.00	0.00	0.00	0.00	0.25	0.00	0.00
36.5	0.00	0.00	0.00	0.20	0.00	0.00	0.00	0.00	0.00	0.00	0.00	1.39	0.00	0.00	0.00	0.00	0.00	0.00	0.00
40.5	0.00	0.00	0.00	0.25	0.00	0.25	0.00	0.25	0.00	0.00	0.00	2.49	0.00	0.00	0.00	0.00	0.00	0.00	0.00
44.5	0.00	0.00	0.00	0.00	0.00	0.00	0.00	0.00	0.00	0.00	0.00	1.97	0.00	0.00	0.00	0.00	0.00	0.00	0.25
48.5	0.00	0.00	0.00	0.00	0.00	0.00	0.00	0.25	0.00	0.00	0.00	0.49	0.00	0.00	0.00	0.00	0.00	0.00	0.00
52.5	0.00	0.00	0.00	0.00	0.00	0.00	0.00	0.00	0.00	0.00	0.00	0.50	0.00	0.00	0.25	0.00	0.00	0.25	0.00
56.5	0.00	0.24	0.00	0.24	0.00	0.00	0.00	0.00	0.00	0.24	0.00	0.47	0.00	0.00	0.00	0.00	0.00	0.24	0.00

Table S8 - NM-16 pollen (percentages)

Depth	POLYGONACEAE UNDIFF.	POLYGONUM AVICULARE TYPE	RUMEX	ARMERIA 'A' LINE	ARMERIA 'B' LINE	CONVOLVULUS	CALYSTEGIA	SCROPHULARIACEAE UNDIFF.	MENTHA TYPE	PLANTAGO MARITIMA TYPE	PLANTAGO MAJOR TYPE	PLANTAGO LANCEOLATA	PLANTAGO CORONOPUS TYPE	SUCCISA TYPE	SCABIOSA	KNAUTIA	BIDENS TYPE	ASTER TYPE	ANTHEMIS TYPE
0.5	0.00	0.00	0.00	0.00	0.34	0.00	0.00	0.00	0.00	0.00	0.00	0.34	0.00	0.00	0.00	0.00	0.00	0.34	0.00
4.5	0.00	0.24	0.00	0.00	0.00	0.00	0.00	0.00	0.00	1.20	0.24	0.48	0.00	0.00	0.00	0.00	0.00	0.00	0.00
8.5	0.00	0.00	0.00	0.00	0.00	0.00	0.00	0.25	0.00	1.30	0.00	1.75	0.25	0.00	0.00	0.00	0.75	0.00	0.00
12.5	0.00	0.00	0.00	0.00	0.00	0.00	0.00	0.00	0.00	7.60	0.25	2.21	0.25	0.25	0.00	0.00	0.25	0.00	0.00
16.5	0.00	0.00	0.00	0.25	0.75	0.00	0.00	0.00	0.00	14.10	0.00	5.03	0.00	0.25	0.00	0.00	0.25	0.00	0.00
20.5	0.00	0.00	0.00	0.25	0.25	0.00	0.25	0.00	0.00	37.00	0.25	2.28	0.00	0.00	0.00	0.00	0.00	0.00	0.00
24.5	0.00	0.21	0.00	0.00	0.21	0.00	0.00	0.00	0.00	25.30	0.84	11.48	0.21	0.00	0.00	0.00	0.63	0.00	0.00
28.5	0.27	0.00	0.00	0.00	0.00	0.00	0.00	0.00	0.00	51.10	3.83	9.02	0.55	0.27	0.00	0.00	0.00	0.00	0.27
32.5	0.00	0.00	0.25	0.25	0.00	0.00	0.00	0.00	0.00	15.60	0.25	34.81	2.47	0.25	0.49	0.00	0.74	0.00	0.00
36.5	0.00	0.00	0.00	0.20	0.00	0.00	0.00	0.00	0.00	0.20	0.00	7.75	0.00	0.20	0.00	0.00	1.79	0.00	1.19
40.5	0.00	0.00	0.25	0.00	0.00	0.00	0.00	0.00	0.00	0.00	0.25	6.23	0.00	0.00	0.00	0.00	0.00	0.00	3.49
44.5	0.00	0.00	0.00	0.00	0.00	0.00	0.00	0.00	0.00	0.00	0.00	1.97	0.00	0.25	0.00	0.25	0.98	0.00	0.00
48.5	0.00	0.00	0.00	0.00	0.00	0.25	0.00	0.00	0.00	0.20	0.00	7.88	0.25	0.00	0.00	0.00	2.46	0.00	0.25
52.5	0.25	0.00	0.00	0.00	0.00	0.00	0.00	0.00	0.25	0.00	0.00	1.24	0.00	0.25	0.00	0.00	1.74	0.00	0.75
56.5	0.00	0.00	0.00	0.00	0.00	0.00	0.00	0.00	0.00	0.00	0.00	2.13	0.00	0.24	0.00	0.00	0.00	0.00	0.24

Table S8 - NM-16 pollen (percentages)

Depth	ARTEMISIA	CIRSIUM TYPE	CENTAUREA NIGRA TYPE	SERRATULA TYPE	LACTUCOIDEAE	POACEAE	CEREAL TYPE	LARGE >45u POACEAE	UNIDENTIFIED/DEGRADED	TRIGLOCHIN MARITIMA	TYPHA ANGUSTIFOLIA TYPE	CYPERACEAE	PTERIDIUM AQUILINUM	DRYOPTERIS TYPE	POLYPODIUM VULGARE	SPHAGNUM	LIVERWORTS	PEDIASTRUM	PRE-QUATERNARY
0.5	0.00	0.00	0.00	0.00	0.00	16.44	0.34	4.11	0.00	1.66	0.00	1.66	0.34	1.35	0.00	0.00	0.00	0.00	0.00
4.5	0.00	0.00	0.00	0.00	0.00	23.15	4.06	7.88	1.67	0.00	0.00	0.71	1.17	0.47	0.00	0.00	0.00	0.24	0.47
8.5	0.00	0.25	0.00	0.25	0.00	28.07	0.25	3.51	0.00	2.54	0.00	5.31	1.47	0.49	0.00	0.00	0.00	0.00	0.00
12.5	0.00	0.00	0.00	0.00	0.00	28.99	0.74	2.46	1.97	1.40	0.70	3.26	1.45	0.00	0.00	0.00	0.00	0.00	0.25
16.5	0.25	0.00	0.00	0.00	1.01	43.22	3.77	4.77	1.01	2.87	0.00	1.91	0.74	0.74	0.00	0.00	0.00	0.74	0.74
20.5	0.00	0.00	0.00	0.00	0.25	42.03	2.53	2.28	0.51	2.40	1.44	1.44	1.00	0.25	0.25	0.00	0.00	1.25	0.25
24.5	0.00	0.00	0.21	0.00	0.21	42.38	0.84	9.39	0.21	0.00	0.00	1.44	0.00	0.00	0.00	0.00	0.00	0.00	0.42
28.5	0.00	0.00	0.27	0.00	3.28	22.13	0.00	1.37	0.27	0.00	0.00	1.08	4.92	0.26	0.00	0.00	0.00	0.00	0.54
32.5	0.00	0.25	0.00	0.00	7.90	26.17	0.49	0.74	0.00	0.00	0.00	2.17	2.63	0.00	0.72	0.00	0.00	0.25	0.00
36.5	0.00	0.40	0.00	0.20	11.33	67.00	0.40	0.60	0.00	0.00	0.00	5.63	1.17	0.20	0.20	0.00	0.00	0.00	0.20
40.5	0.00	0.50	0.00	0.00	9.48	54.86	2.49	1.00	0.50	0.00	0.00	1.72	2.42	0.48	0.00	0.24	0.00	0.00	0.00
44.5	0.00	0.00	0.00	0.00	2.70	56.76	1.47	0.25	2.70	0.00	0.24	2.39	11.02	0.42	2.33	0.00	0.00	0.00	0.00
48.5	0.00	0.74	0.74	0.00	5.91	51.72	0.25	0.00	2.46	0.00	0.00	3.10	7.99	0.43	3.89	0.00	0.00	0.00	0.00
52.5	0.00	0.00	0.50	0.00	9.45	50.25	0.00	0.00	1.74	0.00	0.00	1.23	21.85	0.19	2.26	0.00	0.00	0.00	0.00
56.5	0.00	0.00	0.47	0.00	3.08	59.72	0.00	0.00	0.71	0.00	0.00	0.24	7.76	0.21	3.35	0.00	0.21	0.00	0.00

Table S8 - NM-16 pollen (percentages)

Depth	TREES	SHRUBS	ERICALES	HERBS	MARSH	SPORES	MISC.	POLLEN SUM	TOTAL POLLEN COUNT	Abs. Pollen Freq. Grains/ml	CARBON SPHEROIDS	ANGULAR CHARCOAL
0.5	51.71	1.03	0.00	47.26	3.31	1.68	0.00	292	302	15381	3936	6560
4.5	50.60	1.43	0.00	47.97	0.71	1.64	0.71	419	422	19550	18696	9184
8.5	43.36	2.51	0.25	53.88	7.85	1.97	0.00	399	433	17235	14760	29848
12.5	42.26	4.42	1.23	52.09	5.35	1.45	0.25	407	430	11952	1312	6888
16.5	17.59	3.52	0.25	78.64	4.78	1.49	1.49	398	418	76168	328	3280
20.5	8.10	0.76	0.25	90.89	5.28	1.50	1.50	395	417	71375	656	3280
24.5	5.64	0.84	0.21	93.32	1.44	0.00	0.42	479	486	104873	656	4920
28.5	4.37	1.91	1.09	92.62	1.08	5.18	0.54	366	370	94812	0	3608
32.5	5.43	1.48	1.23	91.85	2.17	3.34	0.25	405	414	141450	328	1968
36.5	4.37	1.99	0.80	92.84	5.63	1.57	0.20	503	533	99331	656	10824
40.5	14.21	3.49	0.00	82.29	1.72	3.14	0.00	401	408	94630	0	32472
44.5	20.88	9.09	0.49	69.53	2.63	13.77	0.00	407	418	90200	328	41000
48.5	12.81	11.82	1.48	73.89	3.10	12.31	0.00	406	419	29365	328	117533
52.5	11.69	8.96	11.94	67.41	1.23	24.29	0.00	402	407	40699	0	164000
56.5	7.58	0.00	24.41	68.01	0.24	11.53	0.00	422	423	82585	0	164000

Table S8 - NM-16 pollen (percentages)

Depth	BETULA	PINUS	ABIES	PICEA	CUPRESSACEAE	ULMUS	QUERCUS	POPULUS	JUGLANS	TILIA (degraded)	ALNUS GLUTINOSA	SORBUS TYPE	PRUNUS TYPE	CORYLUS AVELLANA TYPE	SALIX	HEDERA HELIX	ERICA	RANUNCULACEAE UNDIFF.	RANUNCULUS TYPE
0	3.47	9.68	0.25	0.25	0.00	0.00	23.82	0.00	0.00	0.00	0.25	0.00	0.00	1.74	0.25	0.00	0.00	0.00	0.00
4	1.68	16.50	0.00	0.00	1.01	0.00	12.46	0.00	0.00	0.00	1.01	0.00	0.00	0.34	0.34	0.00	0.00	0.00	0.00
8	0.00	19.44	0.00	0.00	0.00	0.00	13.89	0.00	0.00	0.00	1.39	0.00	0.00	0.00	0.00	0.00	0.00	0.00	1.39
12	0.00	24.39	0.00	0.00	0.00	0.00	14.63	0.00	0.00	0.00	1.22	0.00	0.00	0.00	0.00	0.00	0.00	0.00	0.00
16	0.33	4.98	0.00	0.00	0.33	1.33	7.31	0.00	0.00	0.00	0.00	0.00	0.00	0.33	0.33	0.00	0.00	0.00	0.00
20	1.05	11.23	0.00	0.00	0.00	0.70	8.77	0.35	0.00	0.00	1.05	0.35	0.35	0.35	0.00	0.35	0.35	0.35	0.00
24	0.00	13.76	0.00	0.00	0.00	0.00	1.83	0.00	0.00	0.00	0.00	0.00	0.00	0.92	0.00	0.00	0.00	0.00	0.00
28	1.38	2.76	0.00	0.34	0.00	0.00	6.90	0.00	0.00	0.00	0.69	0.00	0.34	0.34	0.00	0.00	0.00	0.00	0.00
32	0.00	0.00	0.00	0.00	0.00	0.98	6.86	0.00	0.00	0.00	0.00	0.00	0.00	0.98	0.00	0.00	0.00	0.00	0.00
36	0.34	1.70	0.00	0.00	0.00	0.00	3.40	0.00	0.00	0.00	0.00	0.00	0.34	2.04	0.00	0.00	0.00	0.00	0.00
40	0.00	3.16	0.00	0.00	0.00	0.00	5.26	0.00	0.00	0.00	0.00	0.00	0.00	0.00	0.00	0.00	0.00	0.00	0.00
44	0.00	0.98	0.00	0.00	0.00	0.00	8.14	0.00	0.33	0.00	0.98	0.00	0.00	0.33	0.00	0.00	0.00	0.00	0.00
48	0.00	2.94	0.00	0.00	0.00	0.00	0.98	0.00	0.00	0.98	0.00	0.00	0.00	1.96	0.00	0.00	0.00	0.00	0.00
56	0.00	2.97	0.00	0.00	0.00	0.00	7.92	0.00	0.00	0.00	0.00	0.00	0.00	0.99	0.00	0.00	0.00	0.00	0.99
64	1.02	1.02	0.00	0.00	0.00	0.00	2.04	0.00	0.00	0.00	0.00	0.00	0.00	0.00	1.02	0.00	1.02	0.00	0.00

Table S9 - NM-6 pollen (percentages)

Depth	BRASSICACEAE UNDIFF.	HORNUNGIA TYPE	SINAPIS TYPE	CERASTIUM TYPE	FABACEAE	TRIFOLIUM TYPE	ONONIS TYPE	SPERGULARIA TYPE	CHENOPODIACEAE	FILIPENDULA	APIACEAE	RUMEX	ARMERIA 'A' LINE	ARMERIA 'B' LINE	MYOSOTIS	SCROPHULARIACEAE	PLANTAGO MAJOR TYPE	PLANTAGO LANCEOLATA	PLANTAGO MARITIMA TYPE
0	0.99	0.00	0.74	0.00	0.00	0.00	0.00	0.74	22.83	0.00	0.00	0.00	0.00	0.25	0.00	0.00	0.00	0.00	3.72
4	21.89	0.00	0.00	0.00	0.00	0.00	0.00	0.00	13.80	0.00	0.00	0.00	0.00	0.00	0.00	0.34	0.00	0.00	2.69
8	22.22	0.00	1.39	0.00	0.00	0.00	0.00	1.39	1.39	0.00	0.00	0.00	0.00	0.00	0.00	0.00	0.00	0.00	6.94
12	0.00	0.00	0.00	0.00	0.00	0.00	0.00	1.22	4.88	0.00	2.44	1.22	0.00	2.44	0.00	0.00	0.00	1.22	1.22
16	0.33	0.33	0.33	0.00	0.00	0.00	0.33	0.00	3.99	0.00	0.00	0.00	0.00	0.66	0.00	0.00	0.00	0.00	5.65
20	0.35	0.00	0.00	0.00	0.35	0.35	0.00	0.35	3.51	0.00	0.00	0.00	0.00	0.35	0.00	0.00	0.00	1.05	1.05
24	0.92	0.00	0.00	0.00	0.00	0.00	0.00	6.42	27.52	0.00	0.00	0.00	1.83	0.92	0.00	0.00	0.00	0.00	6.42
28	0.34	0.00	0.00	0.00	1.72	0.00	0.00	0.34	2.41	0.00	0.00	0.34	1.72	2.07	0.00	0.34	0.00	0.34	5.17
32	2.94	0.00	0.00	0.98	0.00	0.00	0.00	0.98	1.96	0.00	0.00	0.98	0.00	0.00	0.00	0.00	0.00	0.00	8.82
36	1.70	0.00	0.00	0.00	0.00	0.00	0.00	0.00	1.70	0.00	0.00	0.00	0.00	1.02	0.00	0.00	0.34	2.38	5.10
40	0.00	0.00	0.00	0.00	0.00	0.00	0.00	0.00	1.05	0.00	0.00	0.00	0.00	0.00	1.05	0.00	0.00	3.16	7.37
44	0.00	0.00	0.00	0.00	0.00	0.00	0.00	0.00	2.28	0.00	0.00	0.00	0.00	0.98	0.00	0.00	0.33	3.26	5.54
48	0.00	0.00	0.00	0.00	0.00	0.00	0.00	0.00	6.86	0.00	0.98	0.00	0.00	0.00	0.00	0.00	0.98	6.86	1.96
56	0.00	0.00	0.99	0.00	0.00	0.00	0.00	0.99	0.99	0.99	0.00	0.00	0.00	0.00	0.00	0.00	0.99	8.91	9.90
64	0.00	0.00	0.00	0.00	0.00	0.00	0.00	0.00	13.27	0.00	0.00	0.00	0.00	0.00	0.00	0.00	7.14	6.12	7.14

Table S9 - NM-6 pollen (percentages)

Depth	PLANTAGO CORONOPUS TYPE	BIDENS TYPE	ASTER TYPE	ANTHEMIS TYPE	SENECIO TYPE	CIRSIUM TYPE	CENTAUREA NIGRA TYPE	SERRATULA TYPE	LACTUCOIDEAE	POACEAE	CEREAL TYPE	SECALE CEREALE	LARGE >45u POACEAE	UNIDENTIFIED/DEGRADED	TRIGLOCHIN/POTAMOGETON	TYPHA ANGUSTIFOLIA TYPE	CYPERACEAE	PTERIDIUM AQUILINUM	DRYOPTERIS TYPE
0	0.25	0.00	0.50	0.00	0.25	0.25	0.00	0.00	0.00	21.34	1.24	0.00	5.96	1.24	8.16	0.23	0.23	4.50	0.00
4	0.00	0.00	0.00	0.00	0.00	0.00	0.00	0.00	0.00	19.19	1.68	0.00	5.05	2.02	0.00	0.00	0.34	0.34	0.00
8	0.00	0.00	0.00	0.00	0.00	0.00	0.00	0.00	1.39	23.61	0.00	0.00	1.39	4.17	11.11	0.00	0.00	1.37	0.00
12	0.00	0.00	0.00	0.00	0.00	0.00	0.00	0.00	0.00	41.46	0.00	0.00	3.66	0.00	17.65	0.00	1.96	2.38	0.00
16	0.00	0.00	0.33	0.00	0.00	0.00	0.33	0.00	0.00	66.11	0.33	0.00	5.98	0.33	3.53	0.00	0.00	0.00	0.00
20	0.00	0.35	0.00	0.00	0.00	0.00	0.00	0.35	0.00	59.30	0.35	0.00	7.02	0.00	0.34	1.35	2.36	0.35	0.35
24	0.00	0.00	0.00	0.00	0.00	0.00	0.00	0.00	0.00	37.61	0.00	0.00	1.83	0.00	0.00	0.00	2.68	0.00	0.00
28	0.34	2.41	0.00	0.00	3.79	0.00	0.00	0.00	2.07	57.93	1.03	0.34	4.48	0.00	0.66	0.99	2.64	1.36	0.00
32	0.98	0.98	0.00	0.00	0.00	0.00	0.00	0.00	0.98	56.86	0.00	0.00	14.71	0.00	0.00	0.00	4.67	5.50	0.00
36	0.00	0.68	0.00	0.34	1.02	0.00	0.00	0.34	2.38	67.69	0.34	0.00	6.12	1.02	0.00	0.00	1.67	4.22	0.00
40	0.00	0.00	1.05	1.05	0.00	0.00	0.00	0.00	1.05	58.95	0.00	0.00	13.68	3.16	0.00	0.00	6.86	7.62	0.95
44	0.00	0.00	0.00	0.00	0.00	0.00	0.00	0.00	2.28	66.45	0.33	0.00	5.86	1.95	0.00	0.96	0.32	3.43	0.93
48	0.00	2.94	0.00	0.98	0.00	0.00	0.00	0.00	2.94	56.86	0.00	0.00	9.80	1.96	0.94	0.94	1.89	0.00	0.00
56	0.00	0.99	0.00	0.00	0.00	0.00	0.00	0.00	2.97	50.50	0.00	0.00	4.95	3.96	0.00	0.00	0.00	4.67	0.00
64	0.00	5.10	0.00	0.00	0.00	0.00	0.00	0.00	13.27	38.78	0.00	0.00	3.06	0.00	0.00	0.00	6.67	2.94	0.00

Table S9 - NM-6 pollen (percentages)

Depth	POLYPODIUM VULGARE	SPHAGNUM	LIVERWORT	PEDIASTRUM	DINOFLAGGELLATES	PRE-QUATERNARY	TREES	SHRUBS	HERBS	MARSH	SPORES	MISC.	POLLEN SUM
0	0.00	0.00	0.00	0.00	0.00	0.00	37.72	1.99	60.30	8.62	4.50	0.00	403
4	0.00	0.00	0.00	0.00	0.00	0.34	32.66	0.67	66.67	0.34	0.34	0.34	297
8	0.00	0.00	0.00	0.00	0.00	0.00	34.72	0.00	65.28	11.11	1.37	0.00	72
12	0.00	0.00	0.00	0.00	0.00	0.00	40.24	0.00	59.76	19.61	2.38	0.00	82
16	0.00	0.33	0.00	0.33	0.00	0.33	14.29	0.66	85.05	3.53	0.00	0.99	301
20	0.00	0.00	0.00	1.37	0.00	1.37	23.86	1.05	75.09	4.04	0.70	2.73	285
24	0.00	0.00	0.00	1.77	0.00	1.77	15.60	0.92	83.49	2.68	0.00	3.54	109
28	0.00	0.00	0.00	1.66	0.00	2.32	12.41	0.34	87.24	4.29	1.36	3.97	290
32	0.92	0.00	0.00	0.96	0.00	0.96	7.84	0.98	91.18	4.67	6.42	1.92	102
36	0.32	0.00	0.00	0.00	0.93	8.33	5.78	2.04	92.18	1.67	4.55	9.26	294
40	0.95	0.00	0.00	5.00	0.00	0.00	8.42	0.00	91.58	6.86	9.52	5.00	95
44	0.00	0.29	0.29	3.24	0.29	5.31	10.42	0.33	89.25	1.29	4.36	9.44	307
48	0.97	0.00	0.00	0.93	0.00	3.74	4.90	1.96	93.14	3.77	0.97	4.67	102
56	0.93	0.00	0.00	0.00	0.00	0.00	10.89	0.99	88.12	0.00	5.61	0.00	101
64	0.98	0.00	0.00	0.00	0.00	0.00	4.08	2.04	93.88	6.67	3.92	0.00	98

Table S9 - NM-6 pollen (percentages)